Ab initio molecular dynamics of temporary anions using complex absorbing potentials

Jerryman A. Gyamfi* and Thomas-C. Jagau*

Department of Chemistry, KU Leuven, Celestijnenlaan 200F, B-3001 Leuven, Belgium

E-mail: jerrymanappiahene.gyamfi@kuleuven.be; thomas.jagau@kuleuven.be

Abstract

Dissociative electron attachment, that is, the cleavage of chemical bonds induced by low-energy electrons, is difficult to model with standard quantum-chemical methods because the involved anions are not bound but subject to autodetachment. We present here a new computational development for simulating the dynamics of temporary anions on complex-valued potential energy surfaces. The imaginary part of these surfaces describes electron loss, whereas the gradient of the real part represents the force on the nuclei. In our method, the forces are computed analytically based on Hartree-Fock theory with a complex absorbing potential. *Ab initio* molecular dynamics simulations for the temporary anions of dinitrogen, ethylene, chloroethane, and the five mono- to tetrachlorinated ethylenes show qualitative agreement with experiments and offer mechanistic insights into dissociative electron attachments. The results also demonstrate how our method evenhandedly deals with molecules that may undergo dissociation upon electron attachment and those which only undergo autodetachment.

Graphical TOC Entry
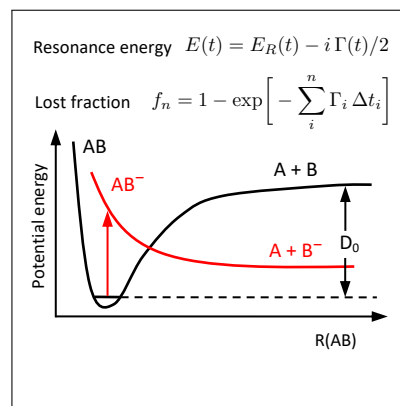
Keywords

complex absorbing potentials, molecular dynamics, temporary anions, electronic resonances, dissociative electron attachment

Temporary anions (TAs)[1,2] are formed when a neutral molecule captures a free electron, most often one with low energy below 10 eV. Albeit their lifetime is in the range of femto- to milliseconds, TAs play a central role in our understanding of important chemical processes: these include DNA lesions in living cells upon exposure to ionizing radiation,[3,4] the formation of radicals and anions in the Earth's atmosphere[5,6] and plasma etching in the semiconductor industry.[7] TAs are also currently reshaping our understanding of the physics and chemistry in interstellar and circumstellar environments.[8]

Studying TAs by means of electronic-structure methods designed for bound states, that is, states related to the discrete spectrum of the electronic Hamiltonian, is difficult, and in many cases a hopeless venture. To begin with, temporary anions are electronic resonances, i.e., metastable states embedded in the continuum of the electronic Hamiltonian.[9–11] Secondly, the formation of a TA may lead to fragmentation of the molecule, which is commonly referred to as dissociative electron attachment (DEA). If DEA is possible, it competes against autodetachment, which makes the computational modeling and prediction of the dissociation channels an intricate problem in its own right.[2,12–14]

Various methods have been proposed to address the difficulties associated with the modeling of TAs and DEA; recent overviews are available in Refs. 10,15. A group of methods combine scattering theory and operator projection techniques,[16–18] for example, the approach by Domcke[19] or the Schwinger multichannel approach by Takatsuka and McKoy.[20] In these methods, an explicit treatment of the continuum is necessary. Recently, Kossoski and co-workers reported an implementation of *ab initio* molecular dynamics (AIMD) for studying TAs.[21] They used bound-state methods to compute the resonance energies and determined the corresponding lifetime using the Schwinger multichannel method.

In this letter, we present a new computational development, dubbed CAP-AIMD, which integrates complex absorbing potentials (CAPs)[22] into AIMD simulations.[23] In our approach, we avoid scattering calculations and obtain the energy and lifetime of a TA as well as the forces acting on the nuclei in a single computation at each time step. As initial applications, we report CAP-AIMD results for the temporary anions of dinitrogen, ethylene, chloroethylene, the three isomers of dichloroethylene, trichloroethylene, tetrachloroethylene, and chloroethane. It is well established that the chlorinated compounds all undergo DEA while dinitrogen and ethylene do not;[14] the CAP-AIMD approach handles both cases evenhandedly.

The fundamental difference between conventional AIMD and CAP-AIMD is that in the latter, the nuclei evolve on a complex potential energy surface (CPES). The CPES is obtained from a non-Hermitian Hamiltonian with complex eigenvalues

$$E = E_r - i\Gamma/2 \,, \tag{1}$$

called Siegert energies.[24] Here, E_r is the energy of a resonance state and Γ its decay width, which is inversely proportional to the lifetime τ. For states, which are electronically bound, $\Gamma = 0$.

In our approach, the CPES is computed on the fly using the CAP method. The CAP Hamiltonian H^η is obtained from the physical Hamiltonian H as[22,25–29]

$$H^\eta = H - i\eta W \,, \tag{2}$$

where η is a real scalar parameter and W is the CAP. We choose W to be quadratic in the electronic coordinate. Mathematical and technical details of this CAP have been discussed elsewhere.[22,26,27,30] The important thing to note here is that W depends on a set of three parameters, $\{r_\alpha^o\}$, $\alpha = x, y, z$, which define its onset. Hence, the CAP is parameterized by the quartet $\{r_\alpha^o, \eta\}$, which needs to be optimized in order to minimize the perturbation of the resonance wave function. In principle, this needs to be redone at each time step as the nuclear configuration changes. We have found, however, that determining the CAP parameters

for the initial structure of the TA and keeping them fixed during the AIMD simulation until the anion becomes bound produces meaningful results. When the anion is bound, η is set to zero. Details on the procedure for determining the optimal quartet $\{r^o_{\alpha,opt}, \eta_{opt}\}$ are discussed in the Supporting Information.

Although it is possible to generate the CPES using other complex-variable techniques,[9,10] we chose here the CAP method because of the availability of analytic gradients.[31,32] Similarly, while one can compute CPES at a higher level of electronic-structure theory, we limit ourselves to Hartree-Fock (HF) theory here because of the computational demands of AIMD simulations. The low level of theory notwithstanding, our CAP-AIMD results show qualitative agreement with experiments and offer insights into the connection between the initial TA and the final DEA products. Questions like, for example, how the molecular orbitals (MOs) of the TA evolve in time may also be answered.

We propagate the nuclei on the CPES according to the classical Hamilton equations

$$\frac{d\mathbf{R}_k}{dt} = \frac{\mathbf{P}_k}{M_k} \tag{3}$$

$$\frac{d\mathbf{P}_k}{dt} = \mathbf{F}_k = -\boldsymbol{\nabla}_k \left(\operatorname{Re} E + V_{nuc-nuc} \right) \tag{4}$$

where $\mathbf{R}_k$, $\mathbf{P}_k$ and M_k are the coordinate, momentum vector and mass of the $k-$th nucleus, and $V_{nuc-nuc}$ is the nuclear repulsion energy. Note that the force $\mathbf{F}_k$ depends on *only* the real part of E. Indeed, if the nuclei are treated classical and nuclear quantum effects are ignored, the force $\mathbf{F}_k$ is simply proportional to the gradient of the real part of the CPES.[33]

After running a CAP-AIMD simulation, one obtains a collection $\{E_n\}$ of complex energies, one for each time step n. The imaginary part of E_n relates to the resonance width Γ_n through Eq. (1). The $\{\Gamma_n\}$ profiles can be used to distinguish TAs, which undergo only autodetachment from those which undergo dissociation. In the first case, Γ oscillates with time, while in the second case it drops to zero at a critical point and stays so indefinitely.

Furthermore, one can estimate from Γ_n the probability P_{n+1} that the TA survives autodetachment between steps t_n and t_{n+1}. Taking Γ_n as the width in the interval $t_n \leq t < t_{n+1}$ leads to the expression

$$P_{n+1} = e^{-\Gamma_n \cdot \Delta t_{n+1}} = e^{-\Delta t_{n+1}/\tau_n} , \tag{5}$$

where $\Delta t_{n+1} = t_{n+1} - t_n$. This probability may be employed to estimate the 'lost fraction', f_n, that is, the fraction of an ensemble of TAs, all characterized by exactly the same initial conditions, statistically expected to undergo autodetachment *by* the time step t_n. In the Supporting Information, we show that

$$f_n = 1 - \prod_{i=1}^{n} P_i = 1 - e^{-\sum_{i=1}^{n} \Gamma_{i-1} \cdot \Delta t_i} . \tag{6}$$

It must be noted that the summation in the exponent in Eq. (6) is an approximation to an integral of Γ over time in the continuous time limit. Hence, for a good estimate of f_n, one needs to choose the time step Δt such that $\Gamma_0 \Delta t < 1$, where Γ_0 is the resonance width at the TA's initial geometry.[34]

For meaningful results, it is paramount to conduct the CAP-AIMD simulation with the desired HF state, meaning the self-consistent field (SCF) solution that corresponds to the resonance and not some discretized continuum state. Indeed, as we show in the Supporting Information, the dynamics of pseudocontinuum states are fundamentally different from those of a resonance. We use the following procedure to find the right SCF solution in the continuum: i) at time step $n = 0$, we build the SCF guess from the core Hamiltonian, then, ii) at any subsequent time step $n > 0$, we use the SCF solution found at the $(n - 1)$-th step as guess. As indicated above, the CAP is turned off as soon as the anion is bound. In order to determine this, we use Koopmans' theorem and consider the real part of the energy of the highest occupied MO (HOMO): If it is negative, we consider the anion to be bound.

To judge how reliable a CAP-AIMD simulation is, we compute in every time step n a deperturbative correction to the complex en-

ergy according to[22,30]

$$\widetilde{E}_n = E_n - \eta \frac{dE_n}{d\eta} = E_n + i\eta \langle W \rangle_n . \quad (7)$$

For a well-represented resonance, $\widetilde{E}_n$ and E_n deviate only little from each other, whereas this is not the case for pseudocontinuum states. Thus, in general, the closer E_n and $\widetilde{E}_n$ are, the better the simulation. Note that the deperturbed lost fraction, $\widetilde{f}_n$, may also be computed by replacing Γ_i in Eq. (6) with $\widetilde{\Gamma}_i = -2 \operatorname{Im} \widetilde{E}_i$.

We implemented our method in the Q-Chem program[35] making use of the implementation of CAP-HF energies[27] and analytic gradients.[31,32] The results reported below should be viewed as proof of concept and as illustration of the robustness of CAP-AIMD simulations. For these reasons, we performed no averaging over initial structures and always took the optimized geometry of the neutral molecule, determined at the HF level, as the initial geometry of the corresponding TA, unless stated otherwise. This is equivalent to a vertical electron attachment at the neutral equilibrium geometry and simulating the time evolution of the formed TA. The cc-pVTZ + 3p basis set with the diffuse p-functions placed on all atoms except hydrogen was used for all simulations and the initial geometry optimizations. Only for tetrachloroethylene, we used aug-cc-pVDZ + 3p instead. The number of trajectories for each TA discussed below ranges between 20 and 200; all ran in the microcanonical ensemble.

The $^2\Pi_g$ shape resonance of N_2^- is an example of a TA which only undergoes autodetachment but does not induce fragmentation.[36] A similar case is the TA of ethylene, for which we report results in the Supporting Information. In Fig. 1, we report resonance widths Γ and lost fractions f for N_2^- from randomly chosen CAP-AIMD trajectories. In Fig. 2, we show the real part of the CPES derived from the same simulations. Cases (A) and (B) in Fig. 1 refer to simulations started at the same initial N-N bond length of 1.067 Å with the same CAP box dimensions but different η values: $\eta = 0.02490$ a.u., which is the optimal η for the initial ge-

ometry, in case (A) and $\eta = 0.00500$ a.u. in case (B). In case (C), we started the simulation at an initial N-N bond length of 1.400 Å, where N_2^- is bound (see Fig. 2) and chose $\eta = 0.00500$ a.u. for the unbound region.

The resonance width has a cyclic profile in all three cases in Fig. 1 because of the vibration of the molecule. We observe a direct correlation between Γ and the N-N bond length. Segments of the Γ profile in Fig. 1 where we see a decrease (increase) correspond to stretching (shortening) of the bond below 1.20 Å, whereas segments with $\Gamma = 0$ correspond to $R_{N-N} \gtrsim 1.20$ Å. When Γ is nonzero, we also see an increase in the lost fraction, whereas it remains constant while $\Gamma = 0$. This suggests that N_2^- is unbound when $R_{N-N} \lesssim 1.20$ Å and that the potential curves of N_2 and N_2^- cross at $R_{N-N} \approx 1.20$ Å according to Koopman's theorem. But Fig. 2 shows that the potential curves cross at $R_{N-N} \approx 1.33$ Å if independent HF calculations are performed for N_2 and N_2^-; in fact, it is known that methods that describe a TA and the neutral molecule with the same Hamiltonian yield a more consistent description.[37] (See Supporting Information for a plot of the imaginary part of the CPES of N_2^-.)

The similarity between cases (A) and (B), which differ only in the η value, indicates some flexibility in choosing this parameter. Overall, we have better agreement between the uncorrected Γ (in red) and the deperturbed $\widetilde{\Gamma}$ (in dark gray) in case (B). Also, the discontinuity at $\Gamma \to 0$ is smaller. However, there is good agreement between the uncorrected (f) and corrected ($\widetilde{f}$) lost fractions in both cases (A) and (B). In case (C), where we start at $R_{N-N} = 1.40$ Å, the lost fraction curve is different from (A) and (B); Γ stays at zero for the first ~ 4.2 fs. In that initial interval, the N-N bond compresses to about 1.2Å. Thereafter, as the N-N bond continues to compress, the autodetachment process ensues and Γ begins to increase. Because the nuclei gain more kinetic energy in case (C) than in (A) and (B), more compressed bond lengths and higher Γ values are reached. Importantly, in all three cases in Fig. 1, f and $\widetilde{f}$ become ~ 1 within 40 fs mean-
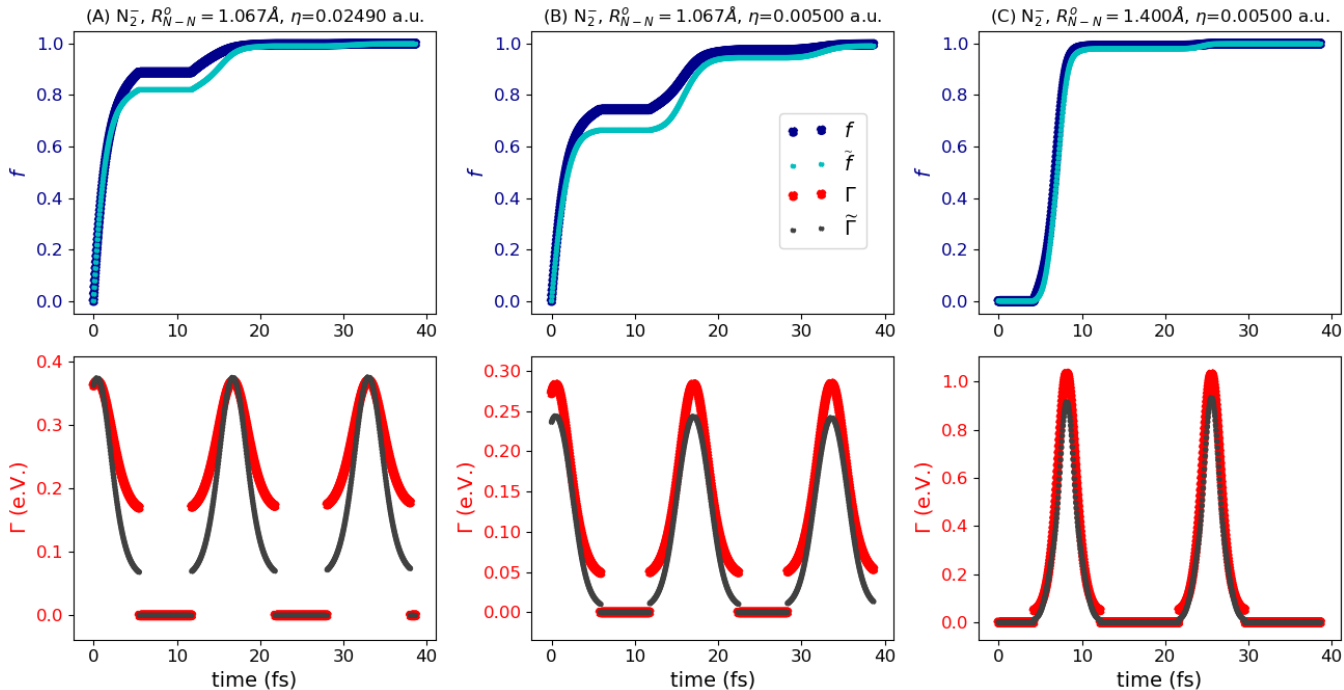
Figure 1: Lost fraction, f, and resonance width, Γ, as well as their deperturbed counterparts, $\widetilde{f}$ and $\widetilde{\Gamma}$, for randomly chosen CAP-AIMD trajectories of N_2^- simulated under different conditions. The profiles are limited to the first 40 fs after vertical electron attachment but Γ and $\widetilde{\Gamma}$ remain periodic in the entire duration of the simulations, which is ~ 140 fs. Time step is 2 a.u. ≈ 0.05 fs.
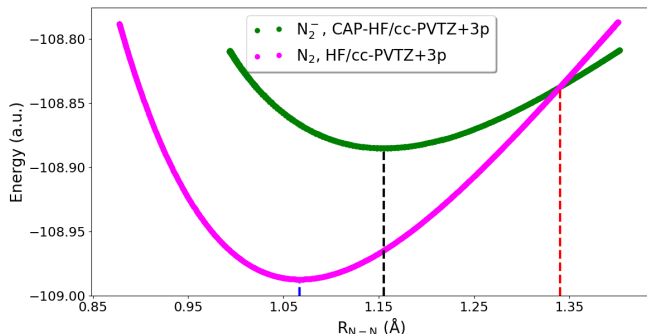
Figure 2: Real part of the CPES of N_2^- (in green) and the PES of N_2 (in magenta). Time step is 2 a.u. ≈ 0.05 fs, total number of time steps is 2000. The curve for N_2 derives from a standard AIMD simulation, while that of N_2^- is from a CAP-AIMD simulation.

ing that it will be very rare to find an anion 40 fs after electron attachment, which is less than 3 vibration periods of neutral N_2.

We now turn our attention to molecules which may undergo DEA. In Fig. 3, we show results from arbitrarily chosen trajectories for the anions of chloroethylene and the three iso-

mers of dichloroethylene. Immediately, we see a stark difference with N_2^-: Γ does not oscillate but falls to zero in less than $\sim$10 fs, during which time we also see a steep rise and stabilization in the lost fraction profile.

Dissociation is possible in all four cases of Fig. 3. The predominant dissociation channel we observe is the formation of Cl^- and an organic radical (see Supporting Information), which is in agreement with experiments.[38] It is worth noting that all TAs become bound before dissociation takes place. The latter is marked by a stabilization of the anion's energy, which becomes discernible when one averages Re E over many trajectories (see Supporting Information). In our simulations, the C-Cl bond cleavage is complete 100-150 fs after electron attachment.

The important differences among the molecules presented in Fig. 3 are the lost fraction profiles, which are determined by two factors (see Eq. (6)): the resonance width and the time it takes a TA to become bound. Both factors relate to the shape of the CPES. In gen-
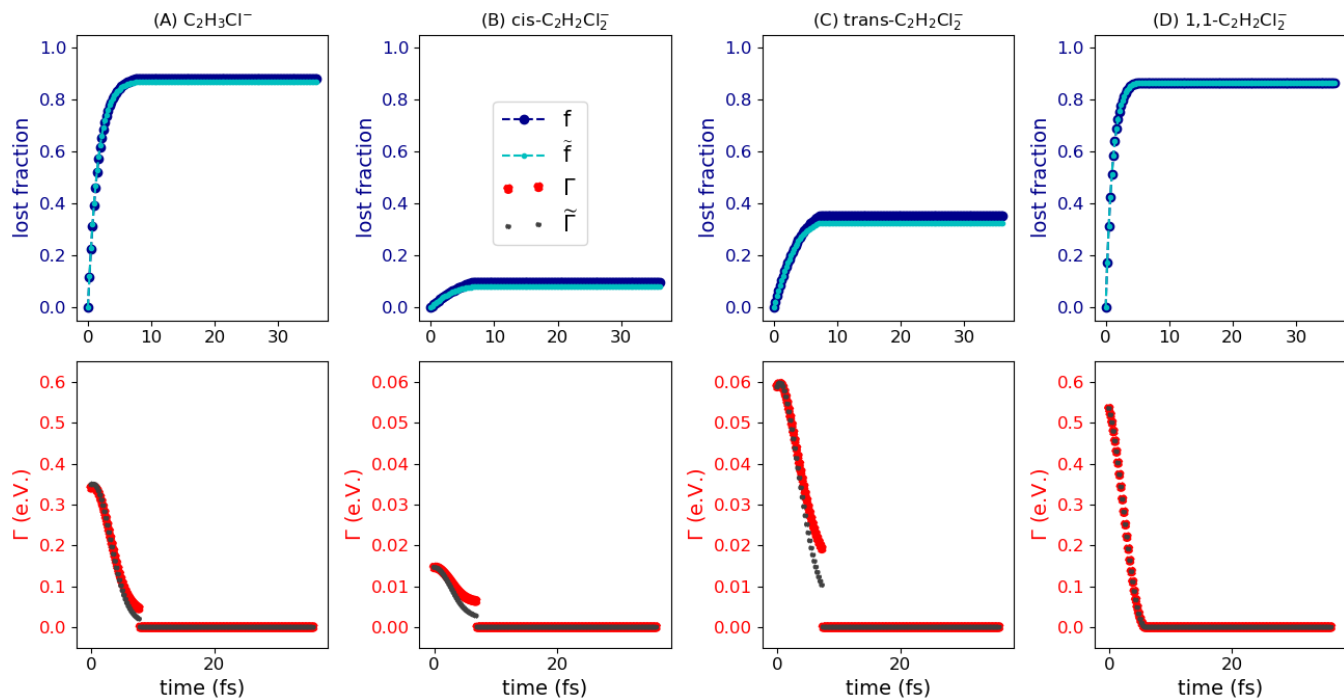
Figure 3: Lost fraction, f, and resonance width, Γ, as well as their deperturbed counterparts, $\widetilde{f}$ and $\widetilde{\Gamma}$, for randomly chosen CAP-AIMD trajectories of the anions of A) chloroethylene, B) *cis-*, C) *trans-* and D) *1,1-* dichloroethylene. The profiles are limited to the first 40 fs.

eral, the closer the initial geometry of the TA is to a bound region on the CPES, the smaller the initial resonance width Γ_0. Also, the more the real part of the gradient at the initial geometry points towards the bound region, the lesser time it will take the TA to reach that region.

Since the bound region is reached very quickly in all four simulations in Fig. 3, Γ_0 is the most important factor in explaining the lost fraction profiles. For the TAs of interest here, Γ_0 decreases in the following order: $CCl_2=CH_2 > CHCl=CH_2 > $ *trans*-$CHCl=CHCl$ > *cis*-$CHCl=CHCl$. The equilibrium lost fractions $f_\infty \equiv \lim_{n\to\infty} f_n$ decreases indeed in the same order. The statistical analysis of our simulations (see Supporting Information) yielded for $\langle f_\infty \rangle$ values of 0.93, 0.92, 0.33, and 0.10 for $CCl_2=CH_2$, $CHCl=CH_2$, *trans*-$CHCl=CHCl$, and *cis*-$CHCl=CHCl$, respectively.

These values allow us to estimate how effective DEA is: For example, for 1,1-dichloroethylene, an average of 7% of the initially formed TAs live long enough for dissociation to happen. For *trans-* and *cis-*dichloroethylene, this average jumps to 67%

and 90%, respectively, resulting in a much larger Cl^- ion yield. This agrees well with experiments,[38] where it was found that the DEA cross section for the Cl^- channel is highest for cis-CHCl=CHCl, followed by *trans*-CHCl=CHCl, and $CH_2=CCl_2$.

The ethylene-derived TAs under discussion here are known to originate from the capture of an electron into the π^* orbital of the C=C bond, giving rise to a $^2\Pi$ anion state.[39,40] According to electron transmission spectroscopy (ETS), DEA proceeds, however, via a $^2\Sigma$ state, which suggests a $^2\Pi \to {}^2\Sigma$ transition mediated by an out-of-plane motion during the C-Cl bond elongation.[39–42] As discussed in the Supporting Information, our CAP-AIMD simulations confirm that.

The $^2\Pi \to {}^2\Sigma$ transition is also evident from the changing character of the HOMO along the trajectory; Fig. 4 illustrates this for the chloroethylene anion. These orbital plots were generated along the trajectory from Fig. 3 (A). It is seen that the HOMO is of π^* character at $t = 0$, while we have mixed π^*-σ^* character at 48 fs. Notably, this plot is very similar to that of
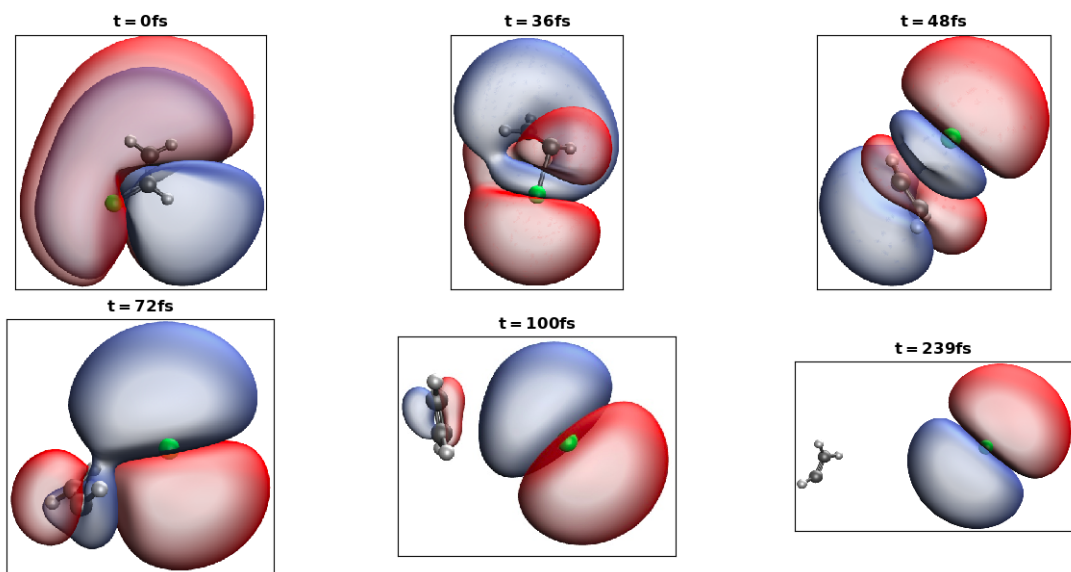
Figure 4: Time evolution of the HOMO of chloroethylene anion. Isovalue is 0.002.

the coupled-cluster Dyson orbital computed at the minimum-energy crossing point between neutral and anionic chloroethylene.[42] Already at 72 fs, the HOMO is largely localized on the Cl atom and the Mulliken charge of this atom is already about -0.9 a.u.

In the Supporting Information, we also report CAP-AIMD results for the anions of trichloroethylene and tetrachloroethylene. Here too, we observe that the $^2\Pi \rightarrow \ ^2\Sigma$ transition is mediated by an out-of-plane motion. For trichloroethylene, we observe four dissociation channels: the three isomers of dichloroethylene together with Cl$^-$, and Cl + C_2Cl^- + HCl. All four channels have been observed in catalyzed reductive dechlorination;[43–45] however, while formation of the *trans*-dichloroethylene radical dominates in our simulations, the experiments all find that the *cis*-dichloroethylene radical is dominant. This discrepancy may be explained by equilibration between the two radicals which is known to happen but it could also be related to stereo- and regioselectivity of the catalysts (e.g., vitamin B_{12}) used in the experiments.[46] We note that our simulations do not take into account any environment and are performed at a low level of theory, i.e., HF. For tetrachloroethylene anion, we observe only the for-

mation of trichloroethylene radical and Cl$^-$, which is consistent with experiments.[43–45] The experiments also find subsequent dechlorination of the trichloroethylene anion formed from the radical yielding the same DEA products discussed in the last paragraph.

To test the CAP-AIMD method for DEA involving only a σ^* resonance, we studied the TA of chloroethane. This is also reported in the Supporting Information; we find an equilibrium lost fraction very close to 1 indicating a small DEA cross-section consistent with experiment[47] and previous theoretical results.[21]

It is worth noting that we did not observe dissociation without a CAP. Such simulations do not capture electron attachment but describe pseudocontinuum states. The notable exception is tetrachloroethylene, whose anion is almost bound at the neutral equilibrium structure making it possible to simulate DEA without a CAP. As shown in the Supporting Information, dissociation is also suppressed when too high or too low CAP strengths are used. Finally, we note that we observed in a small number of trajectories artificial imaginary energies long after the anion has become stable against electron loss. We ignored these artificial imaginary energies in the analysis of the results.

In summary, CAP-AIMD offers a robust method to simulate the dynamics of TAs, independent of whether they undergo dissociation or not. The nuclei are propagated on a complex potential energy surface, yielding a complex energy at each time step, where the imaginary part relates to the decay width of the TA. In addition, the fraction f of TAs lost due to autodetachment can be obtained from CAP-AIMD simulations. The equilibrium value $\langle f_\infty \rangle$ provides a measure for the efficiency of DEA. We conducted CAP-AIMD simulations for the anions of chloroethane and different chlorinated ethylenes; the observed trends in the DEA yield are consistent with experimental results. A remarkable commonality among these simulations is that all anions become stable towards autodetachment after less than 10 fs. We conclude by noting that an obvious challenge for future work is to improve the description of the electronic structure, that is, replacing HF by density functional theory in CAP-AIMD simulations.

Supporting Information Available

Derivation of Eq. (6); information on the CAP parameters used in our simulations and the procedure to determine them; more computational results for all anions studied (dinitrogen, ethylene, chloroethane, chloroethylene, *cis*-dichloroethylene, *trans*-dichloroethylene, *1,1*-dichloroethylene, trichloroethylene, and tetrachloroethylene).

References

(1) Herbert, J. M. The quantum chemistry of loosely-bound electrons. *Rev. Comp. Chem.* **2015**, *28*, 391–517.

(2) Ingólfsson, O., Ed. *Low-Energy Electrons: Fundamentals and Applications*; Pan Stanford Publishing, 2019.

(3) Boudaïffa, B.; Cloutier, P.; Hunting, D.; Huels, M. A.; Sanche, L. Resonant Formation of DNA Strand Breaks by Low-Energy (3 to 20 eV) Electrons. *Science* **2000**, *287*, 1658–1660.

(4) Simons, J. How Very Low-Energy (0.1–2 eV) Electrons Cause DNA Strand Breaks. *Advances in Quantum Chemistry* **2007**, *52*, 171–188.

(5) Rees, M. *Physics and Chemistry of the Upper Atmosphere*; Cambridge Atmospheric and Space Science Series; Cambridge University Press, 1989.

(6) Ranković, M.; Kumar T P, R.; Nag, P.; Kočišek, J.; Fedor, J. Temporary anions of the dielectric gas C_3F_7CN and their decay channels. *J. Chem. Phys.* **2020**, *152*, 244304.

(7) Stoffels, E.; Stoffels, W. W.; Kroesen, G. M. W. Plasma chemistry and surface processes of negative ions. *Plasma Sources Sci. Technol.* **2001**, *10*, 311–317.

(8) Millar, T. J.; Walsh, C.; Field, T. A. Negative Ions in Space. *Chem. Rev.* **2017**, *117*, 1765–1795.

(9) Moiseyev, N. *Non-Hermitian Quantum Mechanics*; Cambridge University Press, 2011.

(10) Jagau, T. C. Theory of electronic resonances: Fundamental aspects and recent advances. *Chem. Commun.* **2022**, *58*, 5205–5224.

(11) Jagau, T.-C.; Bravaya, K. B.; Krylov, A. I. Extending Quantum Chemistry of Bound States to Electronic Resonances. *Annu. Rev. Phys. Chem.* **2017**, *68*, 525–553.

(12) Simons, J. Propensity rules for vibration-induced electron detachment of anions. *J. Am. Chem. Soc.* **1981**, *103*, 3971–3976.

(13) Ásgeirsson, V.; Bauer, C. A.; Grimme, S. Unimolecular decomposition pathways of negatively charged nitriles by ab initio molecular dynamics. *Phys. Chem. Chem. Phys.* **2016**, *18*, 31017–31026.

(14) Fabrikant, I. I.; Eden, S.; Mason, N. J.; Fedor, J. Recent Progress in Dissociative Electron Attachment: From Diatomics to Biomolecules. *Adv. At. Mol. Opt. Phys.* **2017**, *66*, 545–657.

(15) Mašín, Z.; Benda, J.; Gorfinkiel, J. D.; Harvey, A. G.; Tennyson, J. UKRmol+: A suite for modelling electronic processes in molecules interacting with electrons, positrons and photons using the R-matrix method. *Comput. Phys. Commun.* **2020**, *249*, 107092.

(16) Feshbach, H. Unified theory of nuclear reactions. *Ann. Phys.* **1958**, *5*, 357–390.

(17) Taylor, J. *Scattering Theory: The Quantum Theory of Nonrelativistic Collisions*; Dover Books on Engineering; Dover Publications, 2006.

(18) Goldberger, M.; Watson, K. *Collision Theory*; Dover books on physics; Dover Publications, 2004.

(19) Domcke, W. Theory of resonance and threshold effects in electron-molecule collisions: The projection-operator approach. *Phys. Rev.* **1991**, *208*, 97–188.

(20) Takatsuka, K.; McKoy, V. Theory of electronically inelastic scattering of electrons by molecules. *Phys. Rev. A* **1984**, *30*, 1734–1740.

(21) Kossoski, F.; Varella, M. T. d. N.; Barbatti, M. On-the-fly dynamics simulations of transient anions. *J. Chem. Phys.* **2019**, *151*, 224104.

(22) Riss, U. V.; Meyer, H. D. Calculation of resonance energies and widths using the complex absorbing potential method. *J. Phys. B: At. Mol. Opt. Phys.* **1993**, *26*, 4503–4535.

(23) Marx, D.; Hutter, J. *Ab Initio Molecular Dynamics: Basic Theory and Advanced Methods*; Cambridge University Press, 2009.

(24) Siegert, A. J. F. On the Derivation of the Dispersion Formula for Nuclear Reactions. *Phys. Rev.* **1939**, *56*, 750–752.

(25) Sommerfeld, T.; Riss, U. V.; Meyer, H.-D.; Cederbaum, L. S.; Engels, B.; Suter, H. U. Temporary anions - calculation of energy and lifetime by absorbing potentials: the resonance. *J. Phys. B: At. Mol. Opt. Phys.* **1998**, *31*, 4107–4122.

(26) Santra, R.; Cederbaum, L. S. An efficient combination of computational techniques for investigating electronic resonance states in molecules. *J. Chem. Phys.* **2001**, *115*, 6853–6861.

(27) Zuev, D.; Jagau, T.-C.; Bravaya, K. B.; Epifanovsky, E.; Shao, Y.; Sundstrom, E.; Head-Gordon, M.; Krylov, A. I. Complex absorbing potentials within EOM-CC family of methods: Theory, implementation, and benchmarks. *J. Chem. Phys.* **2014**, *141*, 024102.

(28) Dempwolff, A. L.; Hodecker, M.; Dreuw, A. Vertical ionization potential benchmark for unitary coupled-cluster and algebraic-diagrammatic construction methods. *J. Chem. Phys. 156*, 054114.

(29) Gayvert, J. R.; Bravaya, K. B. Projected CAP-EOM-CCSD method for electronic resonances. *J. Chem. Phys.* **2022**, *156*, 094108.

(30) Jagau, T.-C.; Zuev, D.; Bravaya, K. B.; Epifanovsky, E.; Krylov, A. I. A Fresh Look at Resonances and Complex Absorbing Potentials: Density Matrix-Based Approach. *J. Phys. Chem. Lett.* **2014**, *5*, 310–315.

(31) Benda, Z.; Jagau, T.-C. Analytic gradients for the complex absorbing potential equation-of-motion coupled-cluster method. *J. Chem. Phys.* **2017**, *146*, 031101.

(32) Benda, Z.; Rickmeyer, K.; Jagau, T.-C. Structure Optimization of Temporary Anions. *J. Chem. Theory Comput.* **2018**, *14*, 3468–3478.

(33) Moiseyev, N. Forces on nuclei moving on autoionizing molecular potential energy surfaces. *J. Chem. Phys.* **2017**, *146*, 024101.

(34) In our CAP-AIMD simulations for N_2^- where the anion was initially bound, we observed that using the same optimized CAP parameters (with anion at the optimized structure of the neutral), and similar Δt as if the anion was initially unbound, gave good results. This strategy could also work for other anions.

(35) Epifanovsky, E.; Gilbert, A. T. B.; Feng, X.; Lee, J.; Mao, Y.; Mardirossian, N.; Pokhilko, P.; White, A. F.; Coons, M. P.; Dempwolff, A. L. et al. Software for the frontiers of quantum chemistry: An overview of developments in the Q-Chem 5 package. *J. Chem. Phys.* **2021**, *155*, 084801.

(36) Schulz, G. J. Resonances in Electron Impact on Diatomic Molecules. *Rev. Mod. Phys.* **1973**, *45*, 423–486.

(37) Jagau, T.-C.; Krylov, A. I. Complex Absorbing Potential Equation-of-Motion Coupled-Cluster Method Yields Smooth and Internally Consistent Potential Energy Surfaces and Lifetimes for Molecular Resonances. *J. Phys. Chem. Lett.* **2014**, *5*, 3078–3085.

(38) Vasil'ev, Y. V.; Voinov, V. G.; Barofsky, D. F.; Deinzer, M. L. Absolute dissociative electron attachment cross-sections of chloro- and bromo-ethylenes. *International Journal of Mass Spectrometry* **2008**, *277*, 142–150.

(39) Burrow, P.; Modelli, A.; Chiu, N.; Jordan, K. Temporary Σ and Π anions of the chloroethylenes and chlorofluoroethylenes. *Chem. Phys. Lett.* **1981**, *82*, 270–276.

(40) Olthoff, J. K.; Tossell, J. A.; Moore, J. H. Electron attachment by haloalkenes and halobenzenes. *J. Chem. Phys.* **1985**, *83*, 5627–5634.

(41) Clarke, D. D.; Coulson, C. A. The dissociative breakdown of negative ions. *J. Chem. Soc. A* **1969**, 169–172.

(42) Benda, Z.; Jagau, T.-C. Understanding Processes Following Resonant Electron Attachment: Minimum-Energy Crossing Points between Anionic and Neutral Potential Energy Surfaces. *J. Chem. Theory Comput.* **2018**, *14*, 4216–4223.

(43) Neumann, A.; Wohlfarth, G.; Diekert, G. Purification and characterization of tetrachloroethene reductive dehalogenase from Dehalospirillum multivorans. *J. Biol. Chem.* **1996**, *271*, 16515–16519.

(44) Gantzer, C. J.; Wackett, L. P. Reductive dechlorination catalyzed by bacterial transition-metal coenzymes. *Environ. Sci. Technol.* **1991**, *25*, 715–722.

(45) Glod, G.; Angst, W.; Holliger, C.; Schwarzenbach, R. P. Corrinoid-Mediated Reduction of Tetrachloroethene, Trichloroethene, and Trichlorofluoroethene in Homogeneous Aqueous Solution: Reaction Kinetics and Reaction Mechanisms. *Environ. Sci. Technol.* **1997**, *31*, 253–260.

(46) Nonnenberg, C.; van der Donk, W. A.; Zipse, H. Reductive Dechlorination of Trichloroethylene: A Computational Study. *J. Phys. Chem. A* **2002**, *106*, 8708–8715.

(47) Pearl, D. M.; Burrow, P. D. Dissociative attachment in selected monochloroalkanes. *J. Chem. Phys.* **1994**, *101*, 2940–2948.

Supporting Information: *Ab initio* molecular dynamics of temporary anions using complex absorbing potentials

Jerryman A. Gyamfi[*] and Thomas-C. Jagau[*]

Department of Chemistry, KU Leuven, Celestijnenlaan 200F, B-3001 Leuven, Belgium

E-mail: jerrymanappiahene.gyamfi@kuleuven.be; thomas.jagau@kuleuven.be

Lost fraction formula derivation

Following the article, let P_{n+1} be the survival probability of the temporary anion between the $n-$th and $(n+1)$-th steps of the CAP-HF AIMD simulation. Then,

$$\begin{cases} P_0 & = 1 \\ P_{n+1} & = e^{-\Gamma_n \cdot \Delta t_{n+1}}, \qquad n \in \{0, 1, 2 \ldots\}, \end{cases} \tag{1}$$

where $\Delta t_{n+1} \equiv t_{n+1} - t_n$, and $\Gamma_n \equiv -2 \cdot \text{Im } E_n$. E_n is the complex SCF energy at the $n-$th AIMD step. P_0 defines the survival probability *at* the initial instance t_0, and is set to be unity. The probability that we witness autodetachment between the $n-$th and $(n+1)-$th steps, after the temporary anion had survived down to the $n-$th step, is:

$$A_{n+1} = \left[\prod_{i=0}^{n} P_i \right] \cdot (1 - P_{n+1}) \qquad n \in \{0, 1, 2 \ldots\}. \tag{2}$$

We set $A_0 = 0$ since there is no autodetachment at the initial instant t_0.

Consider now an ensemble N of identical temporary anions who share the same initial geometry and initial velocities. It is sufficient to run a single CAP-AIMD simulation for this particular ensemble to obtain the data set $\{\Gamma_n\}$, which informs us of the width of each member of the ensemble along that given trajectory. Without loss of generality, we may take A_{n+1} to be equivalent to the fraction of the initial number N of temporary anions we lose between time steps n and $n + 1$. Thus, the sum

$$f_n \equiv A_0 + A_1 + A_2 + \ldots + A_n \tag{3}$$

is the total fraction lost between time steps 0 and n (included). That is, for $n \geq 1$,

$$f_n = \sum_{m=1}^{n} A_m = \sum_{m=1}^{n} \left[\prod_{i=0}^{m-1} P_i \right] \cdot (1 - P_m), \tag{4}$$

which can be simplified to:

$$f_n = 1 - \prod_{i=1}^{n} P_i = 1 - e^{-1/\hbar \sum_{i=1}^{n} \Gamma_{i-1} \cdot \Delta t_i} \ . \tag{5}$$

There are a number of ways to prove this. We give below a simple proof by induction. Let's begin by writing explicitly the expressions for A_1, A_2:

$$A_1 = (1 - P_1) \tag{6a}$$

$$A_2 = P_1(1 - P_2) = P_1 - P_1 P_2 \tag{6b}$$

Note that $P_1 = 1 - A_1$, and so we may rewrite A_2 as

$$A_2 = 1 - A_1 - P_1 P_2 \tag{7}$$

from which we derive that

$$A_1 + A_2 = 1 - P_1 P_2 \ . \tag{8}$$

If we now consider A_3, we have

$$A_3 = P_1 P_2(1 - P_3) = P_1 P_2 - P_1 P_2 P_3 \ . \tag{9}$$

Since, from Eq. (8), $P_1 P_2 = 1 - A_1 - A_2$, then we may also rewrite Eq. (9) as,

$$A_3 = 1 - A_1 - A_2 - P_1 P_2 P_3 \ , \tag{10}$$

from which we also derive that

$$A_1 + A_2 + A_3 = 1 - P_1 P_2 P_3 \ . \tag{11}$$

3

Following the same line of reasoning, we can see that, in general,

$$\sum_{m=1}^{n} A_m = 1 - \prod_{m=1}^{n} P_i .\qquad(12)$$

Initial molecular structures (Cartesian coordinates in Angstroms)

N2 R_N-N = 1.067 Angstroms:

I	Atom	X	Y	Z
1	N	0.0000000000	0.0000000000	0.0000000000
2	N	0.0000000000	0.0000000000	1.0671420000

N2 R_N-N = 1.400 Angstroms:

I	Atom	X	Y	Z
1	N	0.0000000000	0.0000000000	0.0000000000
2	N	0.0000000000	0.0000000000	1.4000000000

N2 R_N-N = 1.150 Angstroms:

I	Atom	X	Y	Z
1	N	0.0000000000	0.0000000000	0.0000000000
2	N	0.0000000000	0.0000000000	1.1500000000

Ethylene:

I	Atom	X	Y	Z
1	C	0.0000000000	0.0000000000	0.0000000000
2	H	0.0000000000	0.0000000000	1.0742160000
3	H	0.9595703355	0.0000000000	-0.4828713968
4	C	-1.1191466626	0.0000000000	-0.6896850753
5	H	-2.0787169982	0.0000000000	-0.2068136786
6	H	-1.1191466626	0.0000000000	-1.7639010753

```
Chloroethylene:
    I       Atom         X                    Y                    Z
    -----------------------------------------------------------------
    1        Cl       0.0000000000         0.0000000000         0.0000000000
    2        C        0.0000000000         0.0000000000         1.7316720000
    3        H        0.9853392606         0.0000000000         2.1483176034
    4        C       -1.0935317241        -0.0000000000         2.4493744736
    5        H       -2.0698140500        -0.0000000000         2.0064002052
    6        H       -1.0220874542        -0.0000000000         3.5199672631
    -----------------------------------------------------------------


cis-dichloroethylene:
    I       Atom         X                    Y                    Z
    -----------------------------------------------------------------
    1        Cl       0.0000000000         0.0000000000         0.0000000000
    2        C        0.0000000000         0.0000000000         1.7158570000
    3        H        0.9754145626         0.0000000000         2.1546605495
    4        C       -1.0642674138        -0.0000000000         2.4775763725
    5        H       -0.9635098987        -0.0000000000         3.5423909325
    6        Cl      -2.6884303018        -0.0000000000         1.9241686045
    -----------------------------------------------------------------


trans-dichloroethylene:
    I       Atom         X                    Y                    Z
    -----------------------------------------------------------------
    1        Cl       0.0000000000         0.0000000000         0.0000000000
    2        C        0.0000000000         0.0000000000         1.7251020000
    3        H        0.9725182492         0.0000000000         2.1682755046
    4        C       -1.1108641214        -0.0000000000         2.4124445514
    5        H       -2.0833803441        -0.0000000000         1.9692665997
    6        Cl      -1.1108732143         0.0000000000         4.1375455514
    -----------------------------------------------------------------


1,1-dichloroethylene:
    I       Atom         X                    Y                    Z
    -----------------------------------------------------------------
    1        Cl       0.0000000000         0.0000000000         0.0000000000
    2        C        0.0000000000         0.0000000000         1.7223030000
    3        C        1.0985662562         0.0000000000         2.4310014204
    4        H        1.0546069317         0.0008291316         3.5008653643
    5        H        2.0551413131        -0.0005294646         1.9498419721
    6        Cl      -1.5693772271         0.0020344528         2.4319816909
    -----------------------------------------------------------------
```

```
trichloroethylene:
     I      Atom          X                    Y                    Z
   ----------------------------------------------------------------
     1       Cl      0.0000000000         0.0000000000         0.0000000000
     2       C       0.0000000000         0.0000000000         1.7092420000
     3       C       1.0751798641         0.0000000000         2.4583761272
     4       H       0.9959360068         0.0004721400         3.5236907956
     5       Cl      2.6789106202        -0.0002059649         1.8573907787
     6       Cl     -1.5586905277         0.0010844173         2.4407910370
   ----------------------------------------------------------------


tetrachloroethylene:
     I      Atom          X                    Y                    Z
   ----------------------------------------------------------------
     1       Cl      0.0000000000         0.0000000000         0.0000000000
     2       C       0.0000000000         0.0000000000         1.7227670000
     3       C       1.1127702200         0.0000000000         2.4402796195
     4       Cl      2.6820100527        -0.0002426958         1.7293487076
     5       Cl      1.1129142371         0.0003344598         4.1630555810
     6       Cl     -1.5693071217         0.0005641705         2.4335709971
   ----------------------------------------------------------------


chloroethane:
     I      Atom          X                    Y                    Z
   ----------------------------------------------------------------
     1       Cl      0.0000000000         0.0000000000         0.0000000000
     2       C       0.0000000000         0.0000000000         1.7959090000
     3       H       1.0352683828         0.0000000000         2.0949364710
     4       H      -0.4531548755         0.9308229065         2.0949364710
     5       C      -0.7464826193        -1.1936557262         2.3509867800
     6       H      -0.2904814026        -2.1205141302         2.0296230487
     7       H      -1.7794323605        -1.1893612135         2.0296230487
     8       H      -0.7229945558        -1.1560973682         3.4350270623
   ----------------------------------------------------------------
```

CAP box parameters

As mentioned in the article, the CAP Hamiltonian, H^η, is given by[1–5]

$$H^\eta = H - i\eta W , \qquad (13)$$

where H is the physical Hamiltonian, η is a real scalar parameter and W is a Hermitian operator. The potential W was chosen to be quadratic of the following form,

$$W = \sum_{\alpha=x,y,z} W_\alpha , \qquad W_\alpha = \theta(\Delta_\alpha - r_\alpha^o) \cdot (\Delta_\alpha - r_\alpha^o)^2 , \ \Delta_\alpha \equiv |r_\alpha - o_\alpha| \qquad (14)$$

where $\theta(x)$ is a piecewise function defined as

$$\theta(x) \equiv \begin{cases} 1 & \text{if } x > 0 \\ 0 & \text{if } x \leq 0 \end{cases} . \qquad (15)$$

r_α is the electronic coordinate along axis α. The vector (o_x, o_y, o_z) is the origin of the CAP, which in our calculations is chosen to coincide with the center of nuclear charge,[6] that is

$$o_\alpha = \frac{\sum_k R_{k,\alpha} Z_k}{\sum_k Z_k} , \qquad (16)$$

where Z_k and R_k are the charge and coordinate of the $k-$th nucleus, respectively. This choice of o_α allows the origin of the CAP to move with the nuclear frame during the AIMD simulation.

Similar to single point energy CAP calculations, to run a CAP-AIMD simulation, one needs to specify the values of the set $\{r_\alpha^o, \eta\}$, which parameterize the CAP. It has been advocated[4,6,7] to set r_α^o for temporary radical anions equal to the second moment of the neutral molecule's wave function along the axis α, i.e. $r_\alpha^o = \sqrt{\langle r_\alpha^2 \rangle}$. To minimize the perturbation of the resonance wave function by the CAP, one runs an $\eta-$trajectory to

determine an optimal η, i.e. η_{opt}, which is chosen such that[1]

$$\eta_{opt} = \min_{\eta} \left| \eta \frac{dE}{d\eta} \right|. \tag{17}$$

However, in our calculations, we resorted to a more complete approach, whereby the CAP box dimensions, r_α^o, are also optimized. The details of the approach will be expounded on in an upcoming work. For now, it suffices to say that the optimized CAP parameters, $\{r_{\alpha,opt}^o, \eta_{opt}\}$, were chosen according to criterion

$$\{r_{\alpha,opt}^o, \eta_{opt}\} = \min_{\{r_\alpha^o, \eta_{opt}\}} \left| \text{Im} \langle -i\eta W \rangle \right|. \tag{18}$$

The optimized CAP parameters used in our CAP-AIMD simulations are summarized in Tab. 1. The vertical attachment energies (VAE) computed using these parameters are reported in Tab. 2 and compared with results from static CAP-EOM-EA-CCSD calculations taken from Ref. 8. It is interesting to note that the ratio between the CAP-EOM-EA-CCSD VAE's and those from CAP-HF is always between 0.6 and 0.7.

In Tab. 2, we also report values for $|\text{Re} \langle -i\eta W \rangle \,/\, \text{VAE}|$ and $|2\, \text{Im} \langle -i\eta W \rangle \,/\, \Gamma|$ from our CAP-HF calculations. These ratios may be interpreted as relative errors in the computed attachment energies and resonance widths, respectively. The closer they are to zero, the better.

Table 1: CAP parameters optimized at the equilibrium geometry of the neutral molecule, used in the CAP-AIMD simulations. Basis set is cc-pVTZ+3p for all molecules except C_2Cl_4 where aug-cc-pVDZ+3p is used. The extra diffuse functions are placed on all atoms except H.

Molecule	η_{opt}[a]	$r^o_{x,opt}$[b]	$r^o_{y,opt}$	$r^o_{z,opt}$
N_2	2490	3535	3535	8102
C_2H_5Cl	650	3994	4148	4163
C_2H_4	230	4360	2680	4360
C_2H_3Cl	460	8097	4490	16823
cis-$C_2H_2Cl_2$	500	8300	6500	8300
$trans$-$C_2H_2Cl_2$	500	6388	5355	32786
$1,1$-$C_2H_2Cl_2$	10	23800	10856	25131
C_2HCl_3	500	7880	6200	7880
C_2Cl_4	2340	28080	7840	43774

[a] η values are in $\times 10^{-5}$ a.u.
[b] r^o values are in $\times 10^{-3}$ a.u. (bohr).

Table 2: Vertical Attachment Energies (VAE) and resonance widths (Γ) in eV of dinitrogen, chloroethane, ethylene and the mono-, di-, tri- and tetra- chloro-substituted ethylenes computed at the optimized geometry of the neutral molecules with CAP-HF. Values computed with CAP-EOM-EA-CCSD and experimental values are also shown.

Molecule	expt[a]	CAP-EOM-EA-CCSD[b]		CAP-HF			
	VAE	VAE	Γ	VAE	Γ	$\left\|\frac{\text{Re}\langle -i\eta W\rangle}{\text{VAE}}\right\|$	$\left\|\frac{2\,\text{Im}\langle -i\eta W\rangle}{\Gamma}\right\|$
N_2	2.3	–	–	3.396	0.362	$1.91 \cdot 10^{-2}$	$4.08 \cdot 10^{-4}$
C_2H_5Cl	2.35	–	–	4.033	1.488	$2.67 \cdot 10^{-3}$	$1.83 \cdot 10^{-3}$
C_2H_4	1.73	2.155	0.446	2.908	0.661	$2.30 \cdot 10^{-2}$	$1.27 \cdot 10^{-3}$
C_2H_3Cl	1.28	1.730	0.266	2.368	0.341	$4.91 \cdot 10^{-3}$	$1.11 \cdot 10^{-2}$
cis-$C_2H_2Cl_2$	1.11	1.573	0.056	2.158	0.015	$4.41 \cdot 10^{-4}$	$6.32 \cdot 10^{-5}$
$trans$-$C_2H_2Cl_2$	0.80	1.335	0.109	1.942	0.059	$1.68 \cdot 10^{-3}$	$1.26 \cdot 10^{-3}$
$1,1$-$C_2H_2Cl_2$	0.76	1.285	0.245	1.858	0.535	$5.37 \cdot 10^{-6}$	$4.29 \cdot 10^{-4}$
C_2HCl_3	0.59	1.052	0.169	1.637	0.034	$1.48 \cdot 10^{-3}$	$1.12 \cdot 10^{-3}$
C_2Cl_4	0.3	0.982	0.026	1.286	0.007	$8.51 \cdot 10^{-4}$	$8.23 \cdot 10^{-2}$

[a] From Ref. 9.
[b] From Ref. 8.

Results

Below, we show scatter plots related to different specific trajectories in different grades of gray. Average i) real part of the complex SCF energy, ii) resonance width, and iii) lost fraction at each time step are shown in i) dark orange, ii) red, and iii) blue dashed lines, respectively. To make some graphs more intelligible, we plot the related data only for some few initial steps. Unless otherwise stated, the initial geometry is always the optimized geometry of the neutral molecule. All trajectories were run in the microcanonical ensemble; the reported temperatures define the Maxwell-Boltzmann distribution from which the initial velocities were sampled.

Dinitrogen, N_2

The dinitrogen anion was simulated at three different initial geometries: i) $R^o_{N-N} = 1.067$ Å, ii) $R^o_{N-N} = 1.150$ Å and iii) $R^o_{N-N} = 1.400$ Å. The time step chosen for the simulation does not matter as long as the condition $\Gamma_0 \Delta t < 1$ is respected, as explained in the article.

Dinitrogen, N_2, $R^o_{N-N} = 1.067$ Å

Time step = 10 a.u. (0.2419 fs); Number of steps = 1500; Temperature = 300 K; Number of trajectories = 200; $\eta = 0.02490$ a.u.
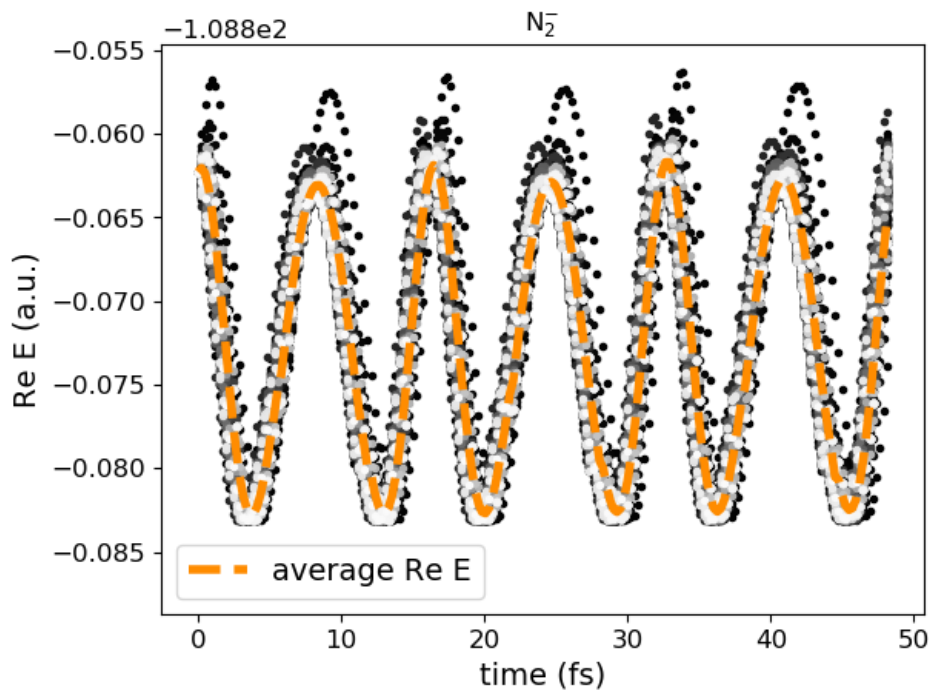
Figure 1: Re E v time for dinitrogen anion. $R^o_{N-N} = 1.067$ Å. An offset of −108.8 is used for the y-axis.
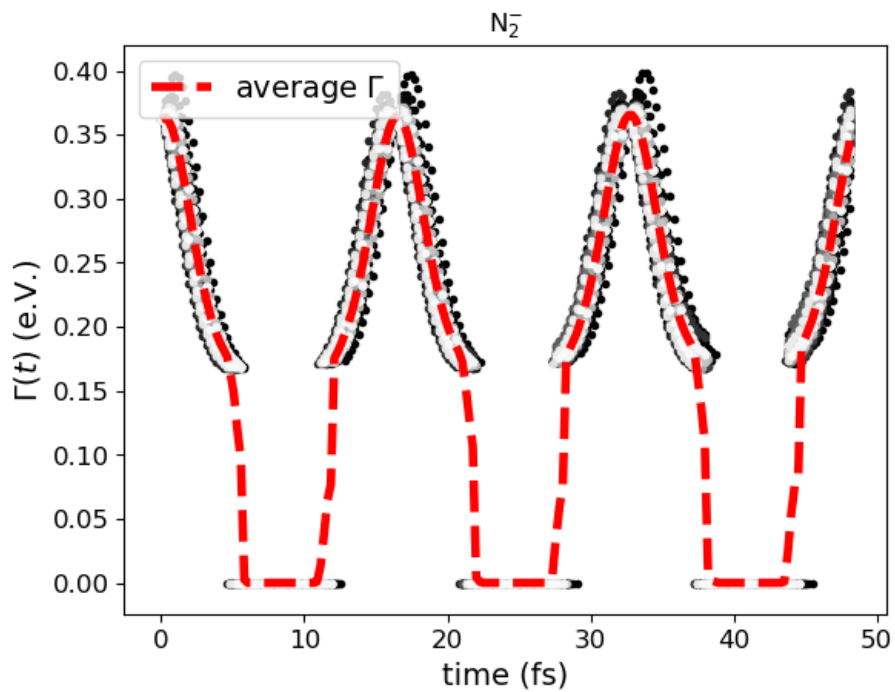
Figure 2: Resonance width, Γ, v time for dinitrogen anion. $R^o_{N-N} = 1.067$ Å
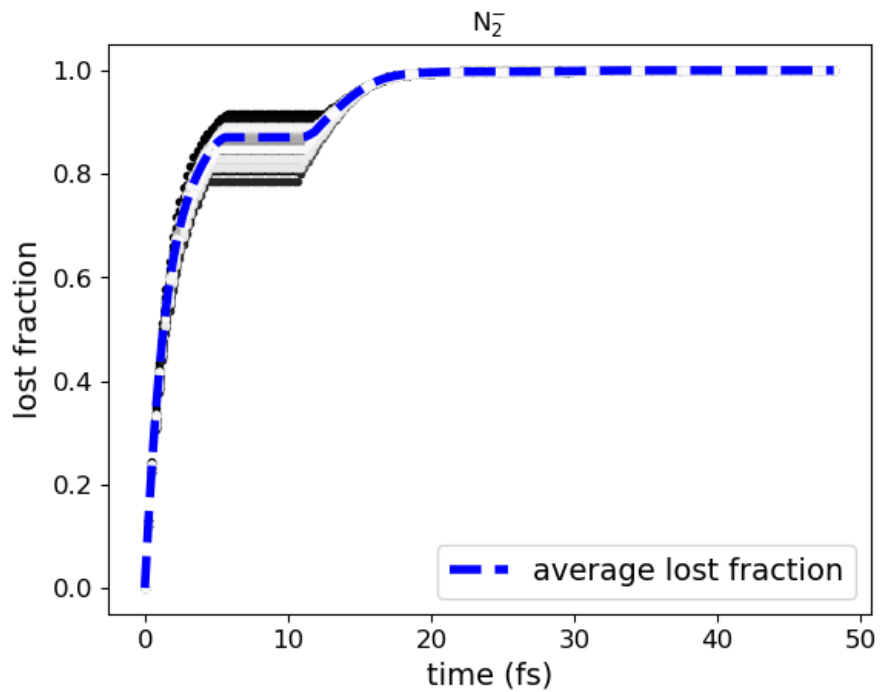
Figure 3: Lost fraction v time for dinitrogen anion. $R^o_{N-N} = 1.067\text{Å}$. The equilibrium lost fraction is 1.0 for all trajectories.

Dinitrogen, N_2, $R^o_{N-N} = 1.400$ Å

Time step = 2 a.u. (0.0484 fs); Number of steps = 2000; Temperature = 300 K; Number of trajectories = 40; $\eta = 0.00500$ a.u.
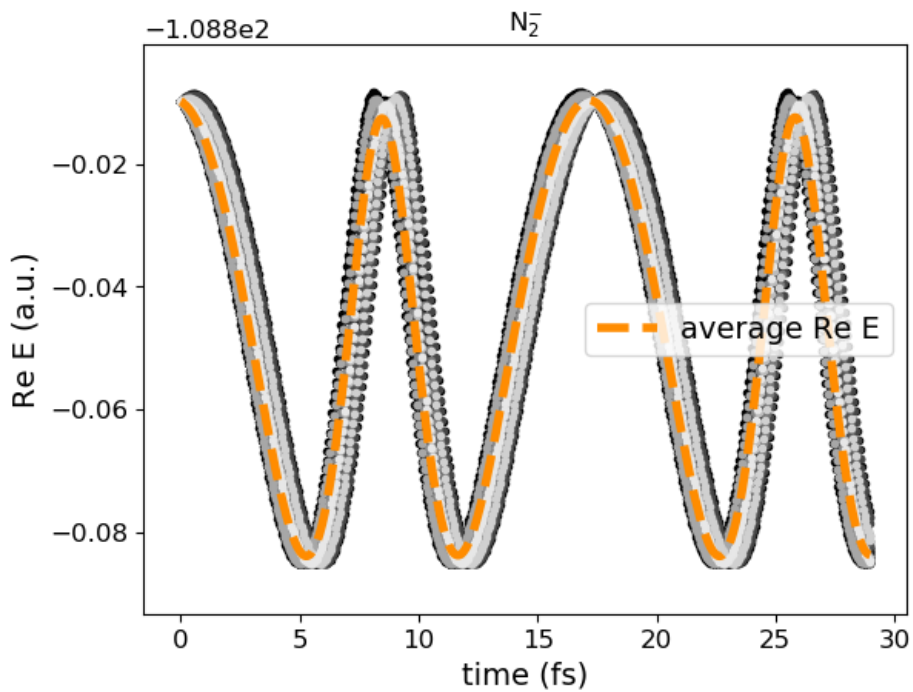
Figure 4: Re E v time for dinitrogen anion. $R^o_{N-N} = 1.400$Å. An offset of -108.8 is used for the y-axis.
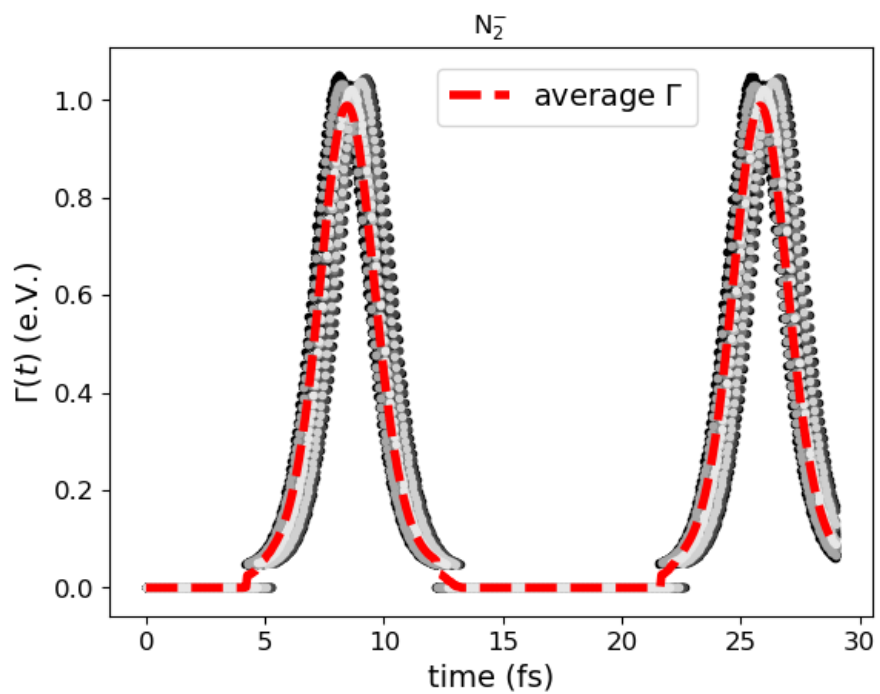
Figure 5: Resonance width, Γ, v time for dinitrogen anion. $R^o_{N-N} = 1.400$ Å
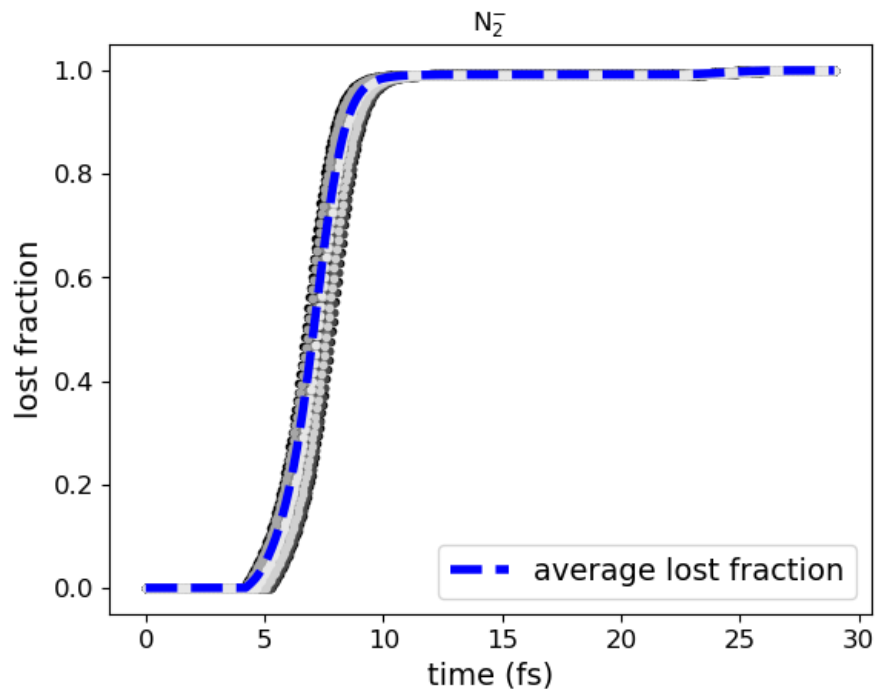
Figure 6: Lost fraction v time for dinitrogen anion. $R^o_{N-N} = 1.400$ Å. The equilibrium lost fraction is 1.0 for all trajectories.

Dinitrogen, N_2, $R^o_{N-N} = 1.150$ Å.

Time step = 2 a.u. (0.0484 fs); Number of steps = 2000; Temperature = 300 K; Number of trajectories = 51; $\eta = 0.00070$ a.u.

We can see in these simulations that the Γ time profile (Fig. 8) is not uniform as in the other initial geometries of the same anion considered above; in particular, it could increase or decrease in the beginning. This is related to the high dependence of Γ on the initial velocities at this initial geometry, which is in the neighborhood of the anion's equilibrium structure. The plot of the real part of the complex SCF energy, Re E, against time (Fig. 7) also shows a small difference between the maxima and minima of the peaks compared to the other initial geometries considered above. Just like the Γ profile (Fig. 8) the lost fraction time profile also shows less homogeneity compared to Figs. 3 and 6.
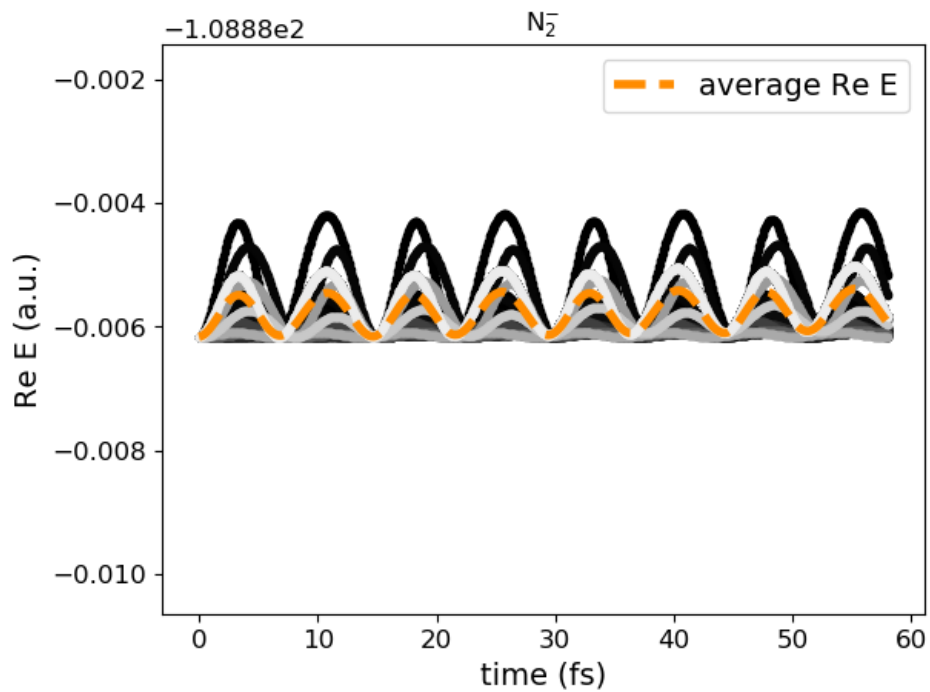
Figure 7: Re E v time for dinitrogen anion. $R^o_{N-N} = 1.150$ Å. An offset of −108.8 is used for the y-axis.
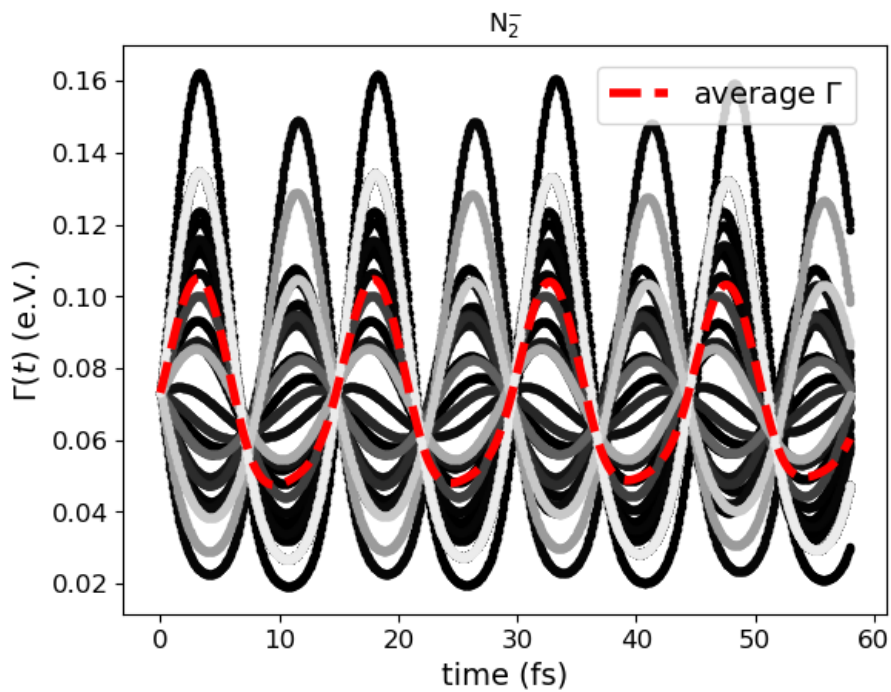
Figure 8: Resonance width, Γ, v time for dinitrogen anion. $R^o_{N-N} = 1.150$ Å.
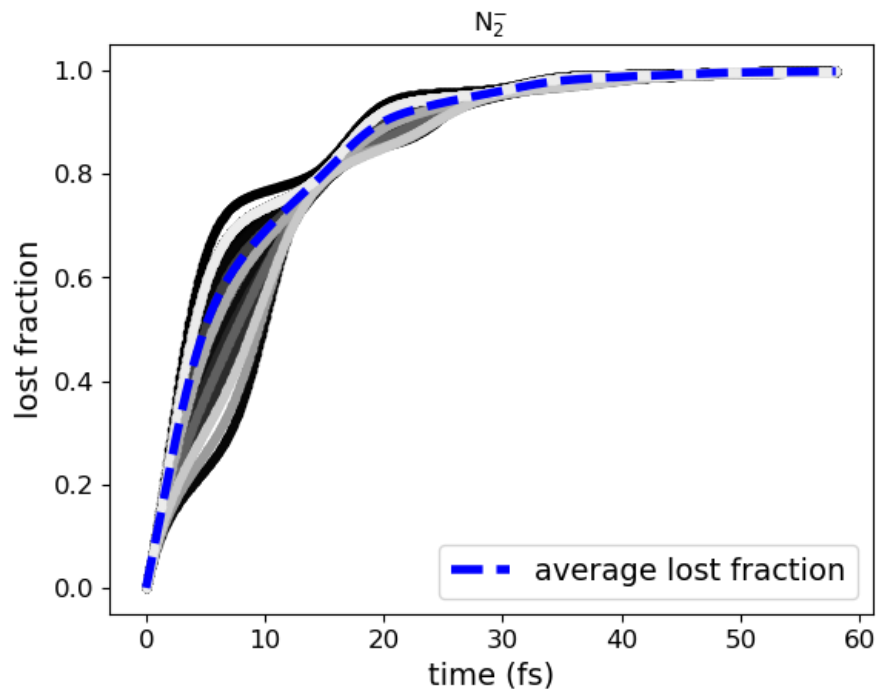
Figure 9: Lost fraction v time for dinitrogen anion. $R^o_{N-N} = 1.150$ Å. The equilibrium lost fraction is 1.0 for all trajectories.

Dinitrogen, variation of Γ with N-N bond length

In Fig. 2 of the article, we reported the real part of the CPES of N_2^- obtained from CAP-AIMD simulation. We now report in Fig. 10 the imaginary part of the same CPES.

Starting from the compressed N-N bond length of $R_{N-N} \sim 1.0$Å, we see that Im E increases as R_{N-N} increases. The upper limit of Im E is zero, which is associated to bound N_2^-.

We observe in Fig. 10 a discontinuity in Im E as Im $E \to 0$, which is around $R_{N-N} \approx$ 1.2Å. The discontinuity is an indication of the transition between bound and unbound N_2^-. It is also a consequence of the limitations of the CAP-HF method.
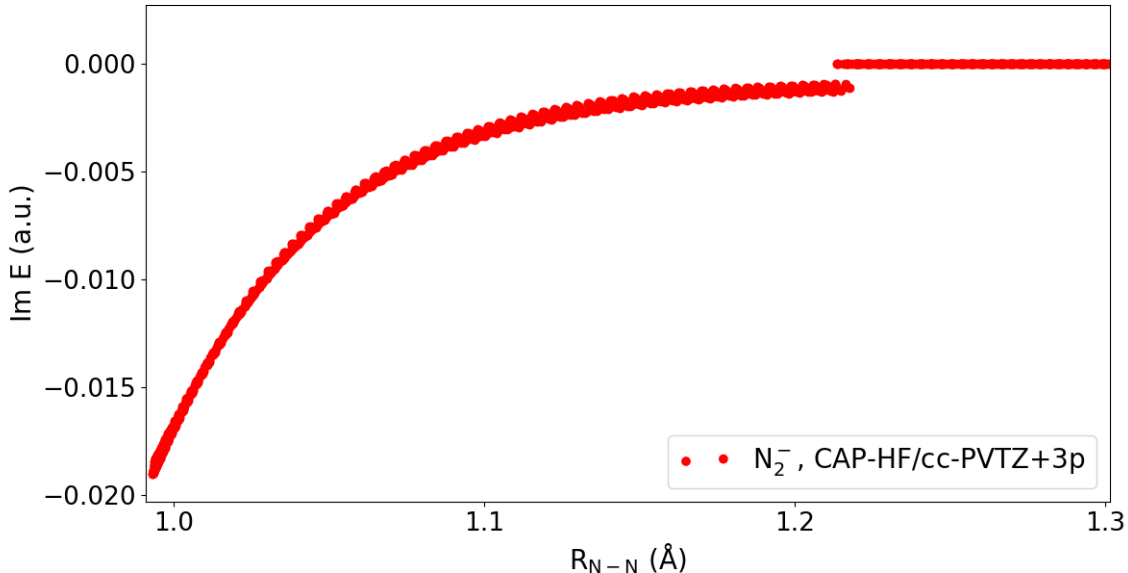
Figure 10: The plot shows variation of the imaginary part of the CPES of N_2^- with N-N bond length, R_{N-N}. The points derive from a CAP-AIMD simulation performed at a time step of 2 a.u. ≈ 0.05 fs, for a total of 2000 time steps.

Ethylene, C_2H_4

Time step = 5 a.u. (0.1209 fs); Number of steps = 1000; Temperature = 200 K; Number of trajectories = 200; $\eta = 0.00230$ a.u.

Looking at the actual trajectories (in shades of gray) in Fig. 12, we see that Γ becomes zero intermittently, indicating the extra electron has become bound; the average Γ (in red) on the other hand, never becomes zero. This is due to the large variance among the trajectories in regards to the Γ profile. However, as we can see from Fig. 13, there is a great homogeneity among the trajectories in regards to the lost fraction's time profile. This is due to the high homogeneity we see in the Γ profiles in the first 10fs.
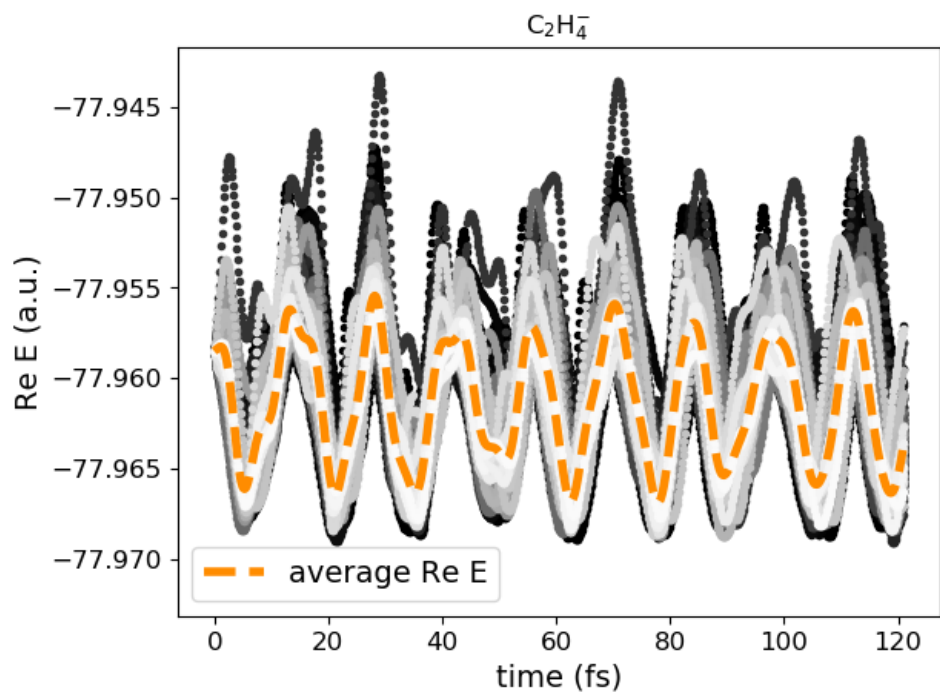
Figure 11: Re E v time for ethylene anion.
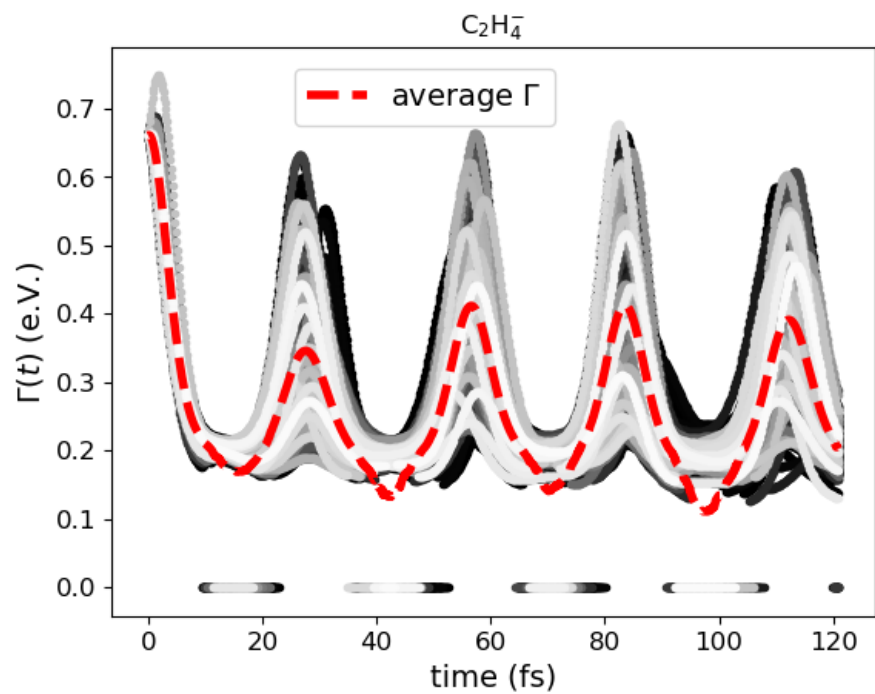
Figure 12: Resonance width, Γ, v time for ethylene anion.
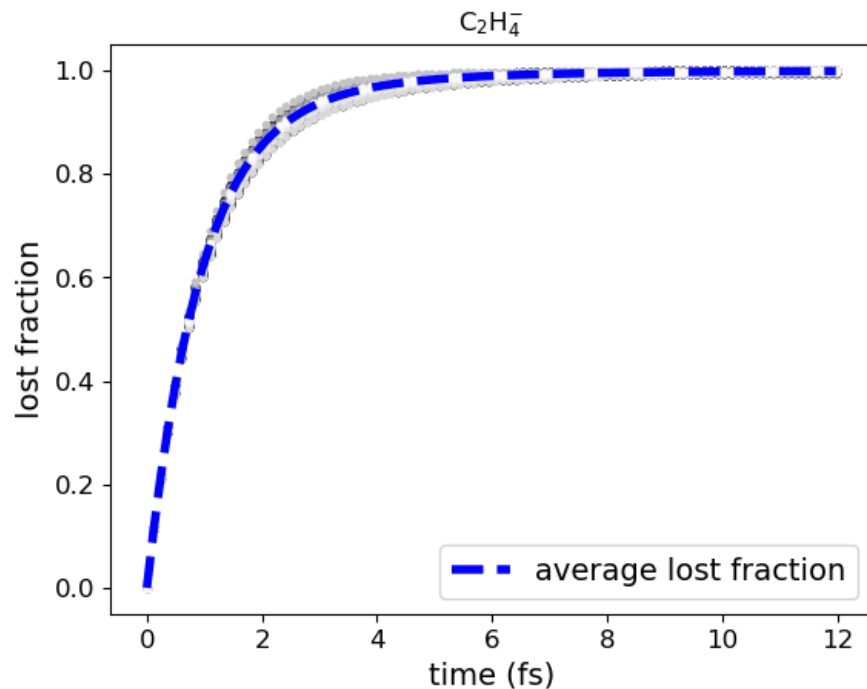
Figure 13: Lost fraction v time for ethylene anion. The equilibrium lost fraction is 1.0 across all trajectories.

Chloroethylene, C_2H_3Cl

Time step = 10 a.u. (0.2419 fs); Number of steps = 1000; Temperature = 300 K; Number of trajectories = 200; $\eta = 0.00460$ a.u.

Statistics on equilibrium lost fraction: *minimum*= 0.7480; *maximum*=0.9973; *mean* =0.9220; *median*=0.9305; *standard deviation* = 0.0416.

In all trajectories, we observe an initial stage where Γ decreases as the nuclei relax. In some trajectories, that stage is followed by a stage where Γ increases again due to the nuclear configurations reached, before eventually becoming zero; this gives rise to the curve centered around 25 fs in Fig. 15.
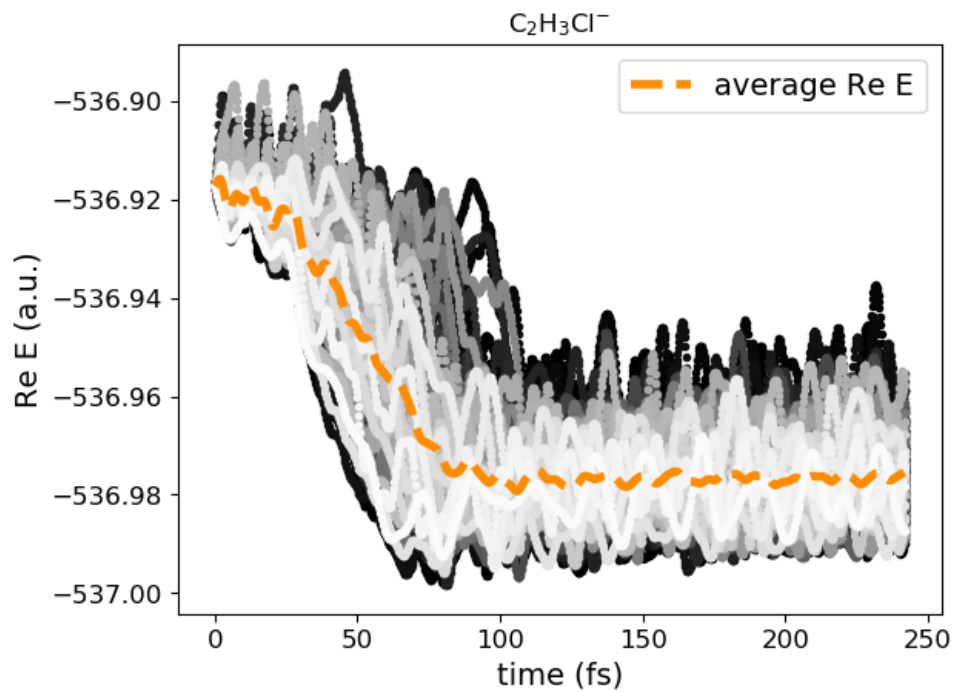
Figure 14: Re E v time for chloroethylene anion.
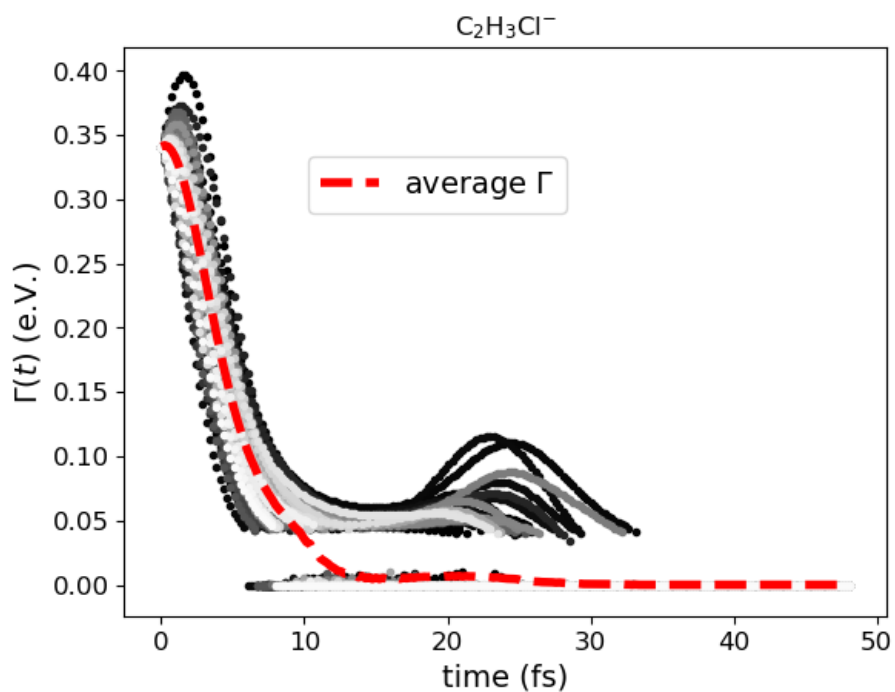
Figure 15: Resonance width, Γ, v time for chloroethylene anion.
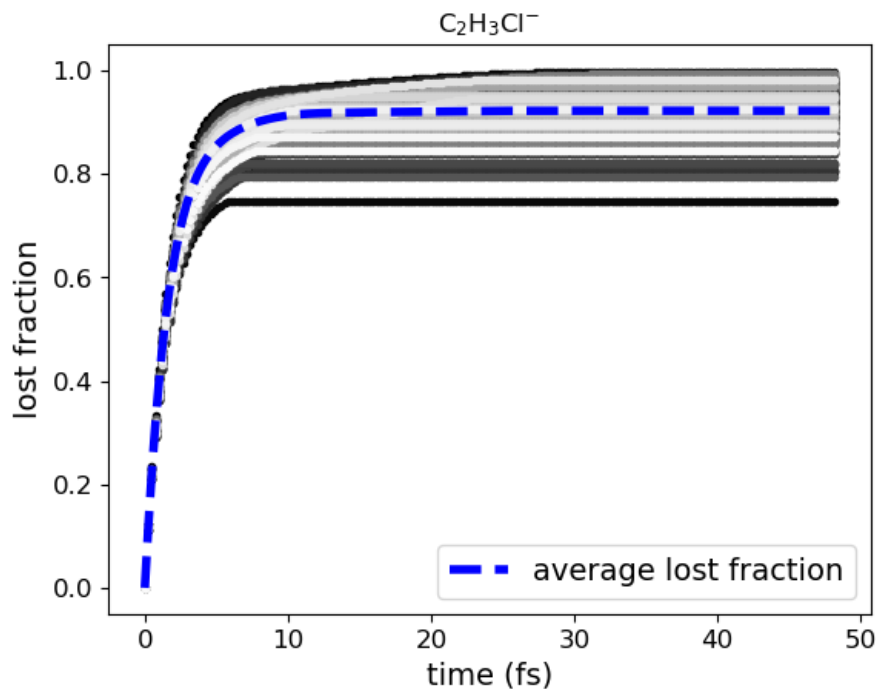
Figure 16: Lost fraction v time for chloroethylene anion.

What happens when the wrong CAP parameters are used?

To illustrate that it is important to run CAP-AIMD simulations with the right CAP parameters, we show below results for chloroethylene anion using the same initial geometry and CAP box parameters used for the simulations above (and listed in Tab. 1), but this time with $\eta = 0.010$ a.u. We chose this value for η because the $\eta-$trajectory (with the same box dimensions as in Tab. 1) indicates that the electronic state of the anion at this η value has pseudocontinuum character and is not a resonance.

Fig. 17 and 18 show disagreement between Re E, Γ and their respective deperturbed counterparts. In Fig. 20, we show as a counterexample, the Re E and Re $\tilde{E}$ values for the trajectories discussed in Fig. 3 of the article; in Fig. 21 we also show the Re E and Re $\tilde{E}$ values for the trajectories discussed in Fig. 1 of the article for N_2^-. The neat agreement between Re E, Γ and their respective deperturbed counterparts in Fig. 20 and 21 is in sharp contrast to what we see in Fig. 17 and 18.
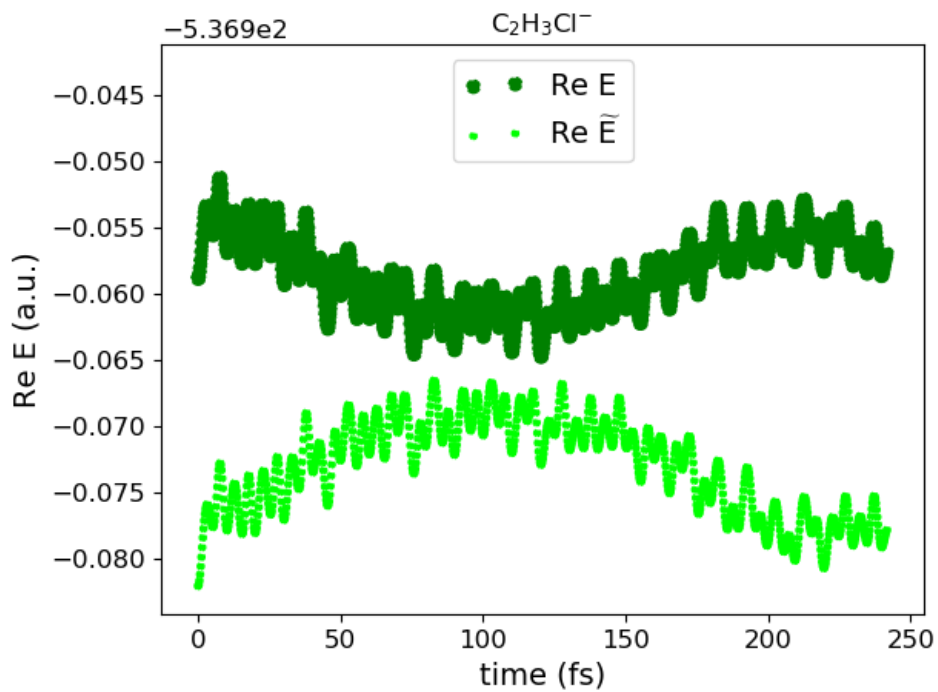
Figure 17: Re E and Re $\widetilde{E}$ v time for chloroethylene anion using $\eta = 0.010$ a.u. An offset of −536.9 is used for the y-axis.
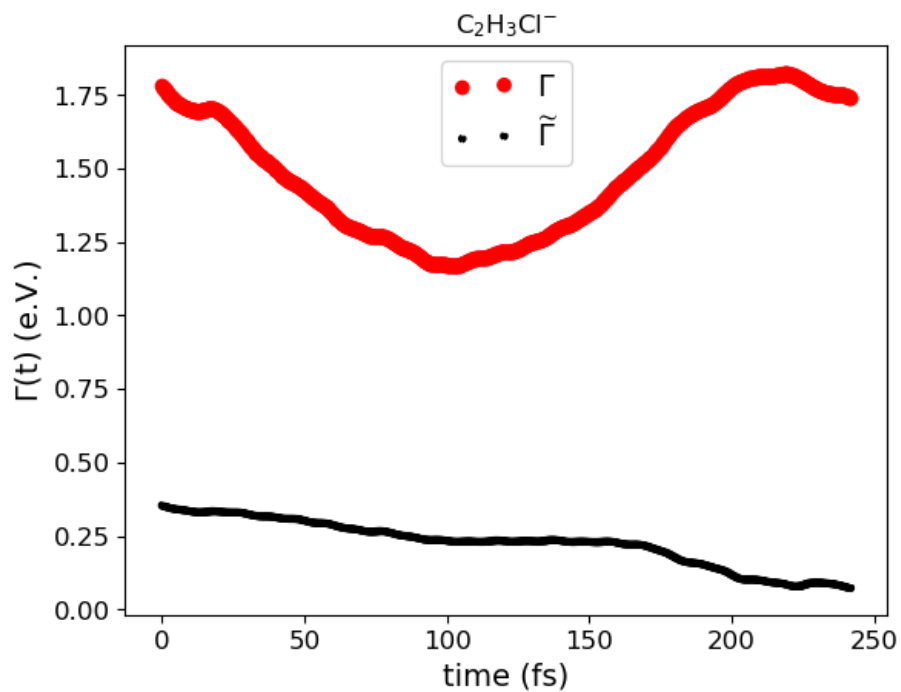
Figure 18: Γ and $\widetilde{\Gamma}$ v time for chloroethylene anion using $\eta = 0.010$ a.u.
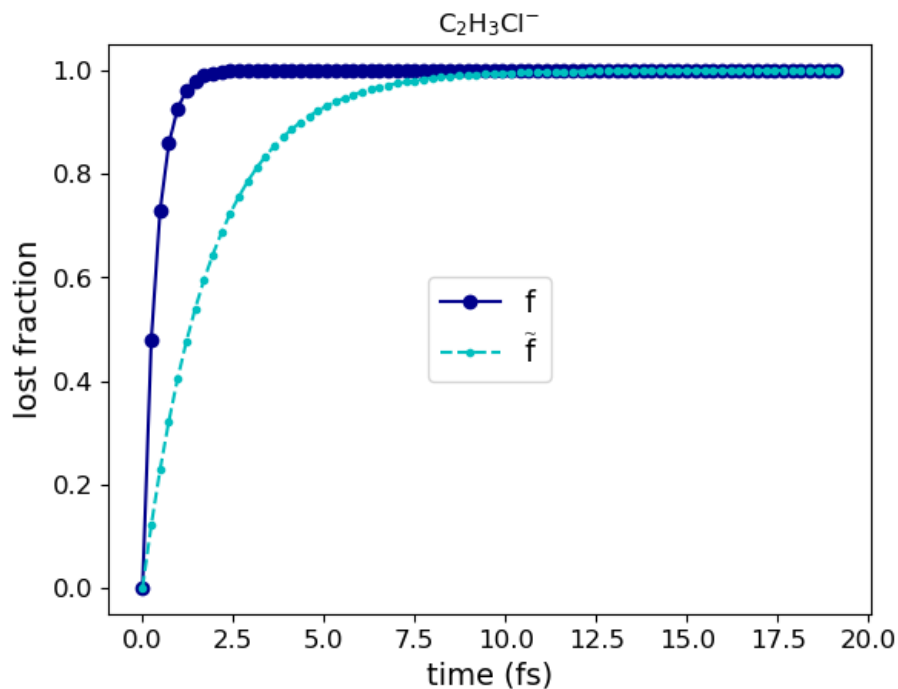
Figure 19: Lost fraction f and deperturbed $\widetilde{f}$ v time for chloroethylene anion using $\eta = 0.010$ a.u.
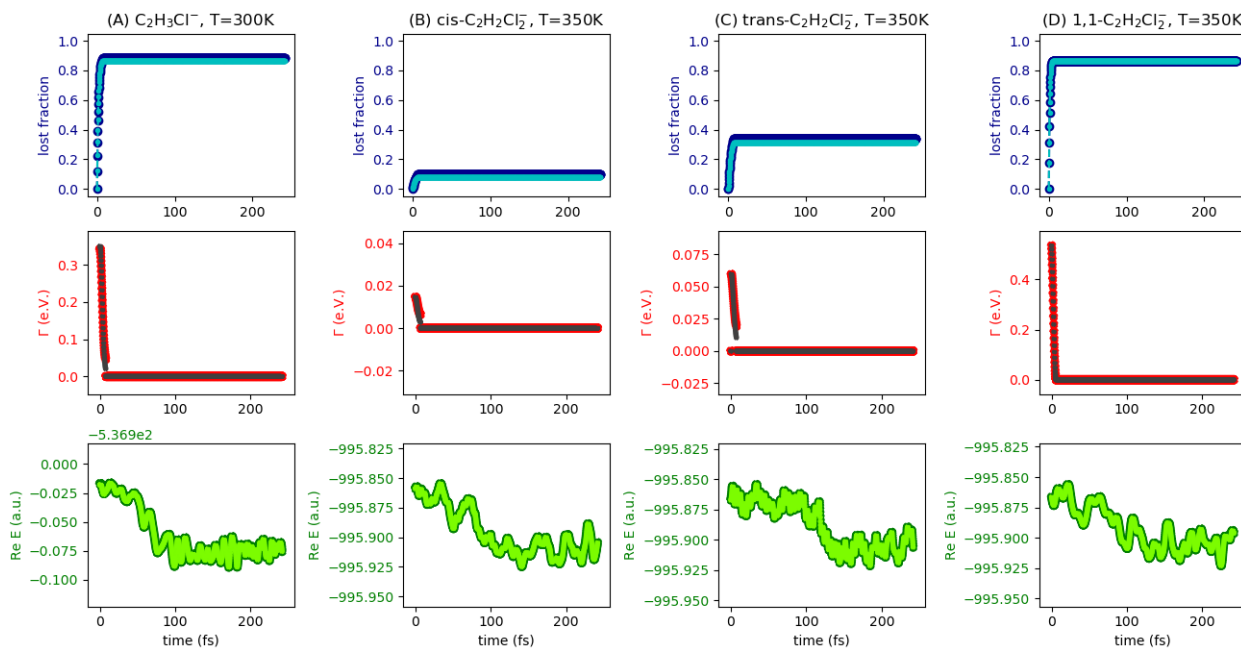
Figure 20: Lost fraction, f, Re E and resonance width, Γ, profiles and their deperturbed counterparts, $\widetilde{f}$, Re $\widetilde{E}$ and $\widetilde{\Gamma}$ for randomly chosen CAP-AIMD trajectories of A) chloroethylene, B) *cis-*, C) *trans-* and D) *1,1*-dichloroethylene anions, simulated with the appropriate CAP parameters from Tab. 1.
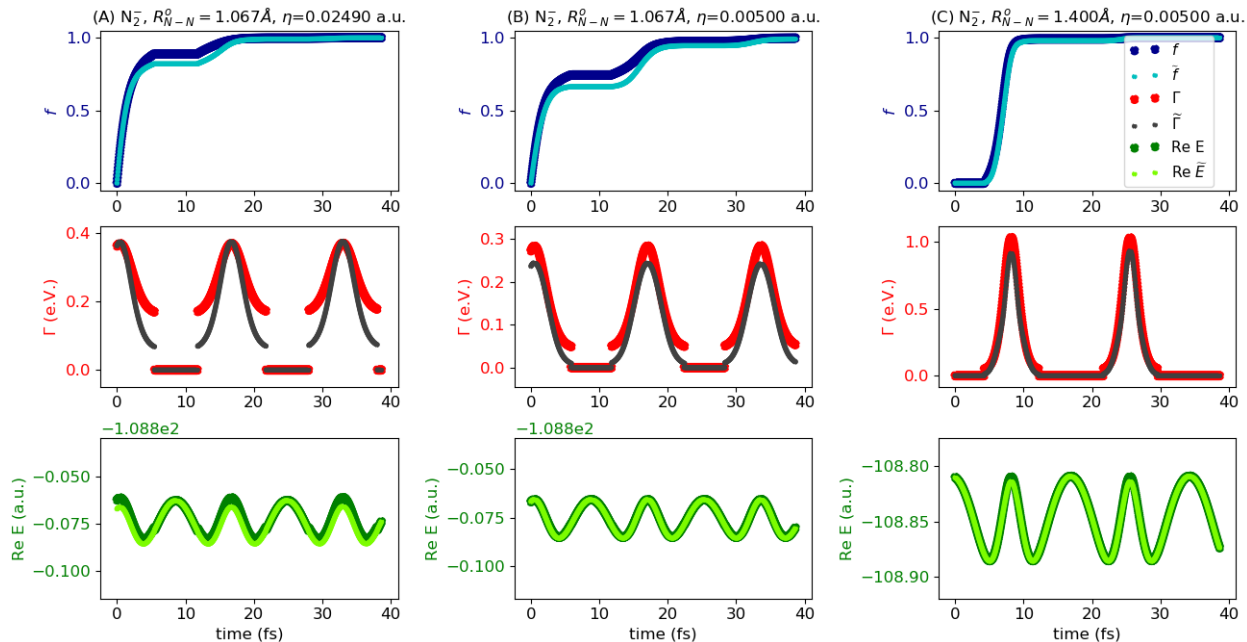
Figure 21: Lost fraction, f, Re E and resonance width, Γ, profiles (and their deperturbed counterparts, $\widetilde{f}$, Re $\widetilde{E}$ and $\widetilde{\Gamma}$) for randomly chosen CAP-AIMD trajectories of N_2^-, simulated with the appropriate CAP parameters from Tab. 1.

cis-dichloroethylene, $C_2H_2Cl_2$

Time step = 10 a.u. (0.2419 fs); Number of steps = 1000; Temperature = 350 K; Number of trajectories = 199; $\eta = 0.00500$ a.u.

Statistics on equilibrium lost fraction: *minimum*= 0.0606; *maximum*=0.1736; *mean* =0.0995; *median*=0.0981; *standard deviation* = 0.0168.
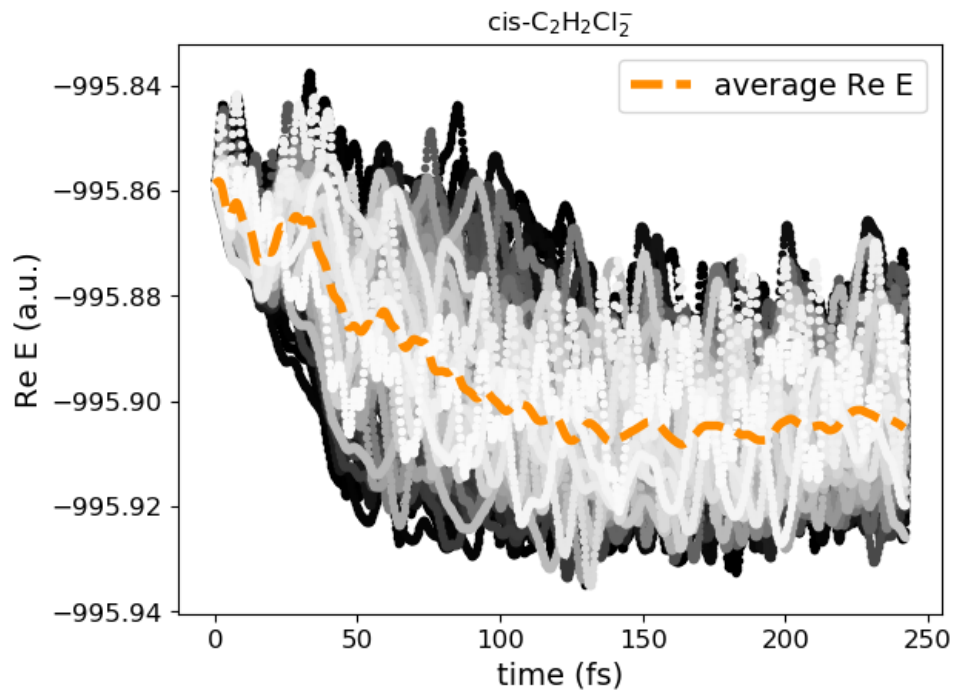
Figure 22: Re E v time for *cis*-dichloroethylene anion.
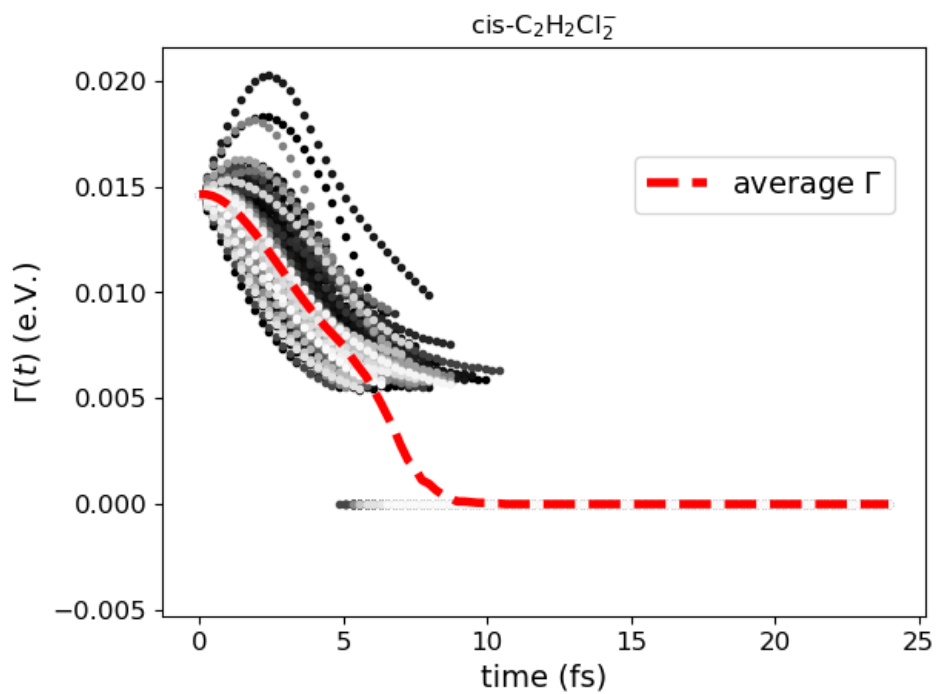
Figure 23: Resonance width, Γ, v time for *cis*-dichloroethylene anion.
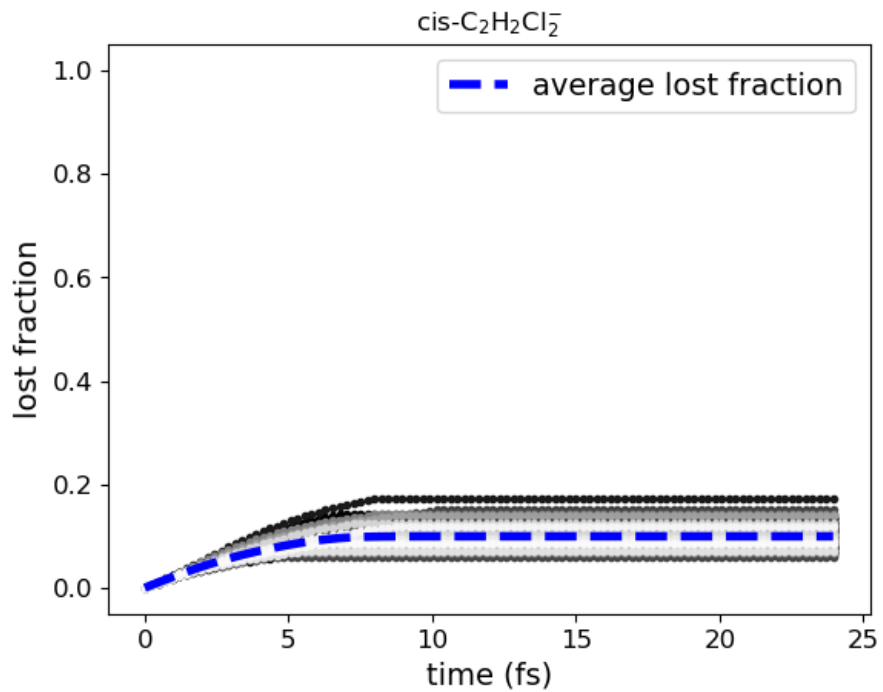
Figure 24: Lost fraction v time for *cis*-dichloroethylene anion.

trans-dichloroethylene, C$_2$H$_2$Cl$_2$

Time step = 10 a.u. (0.2419 fs); Number of steps = 1000; Temperature = 350 K; Number of trajectories = 200; $\eta = 0.00500$ a.u.

Statistics on equilibrium lost fraction: *minimum*= 0.2089; *maximum*=0.4473; *mean* =0.3264; *median*=0.3294; *standard deviation* = 0.0503.
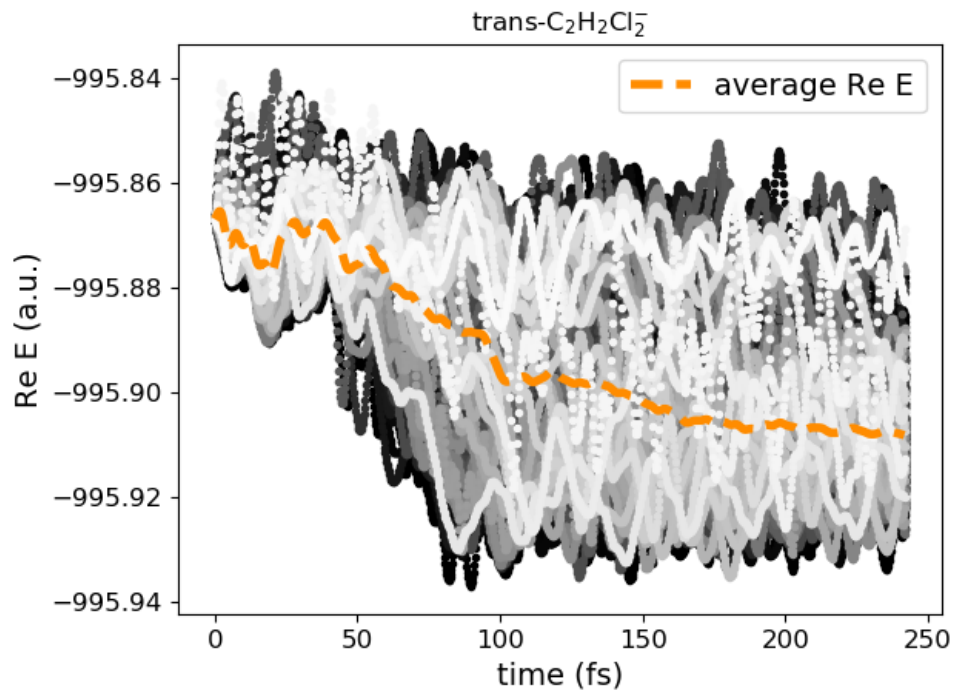
Figure 25: Re E v time for *trans*-dichloroethylene anion.
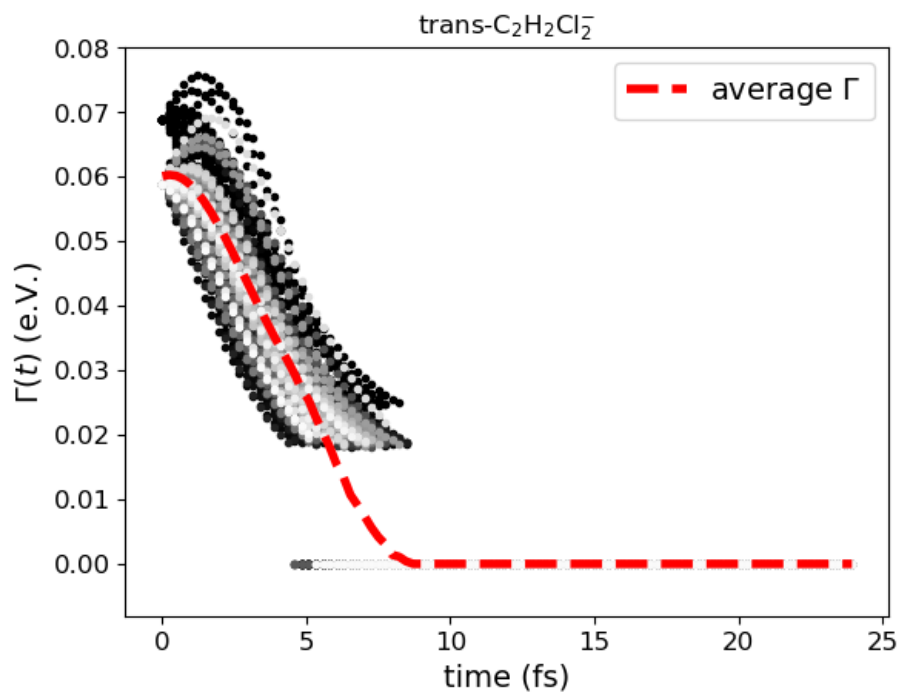
Figure 26: Resonance width, Γ, v time for *trans*-dichloroethylene anion.
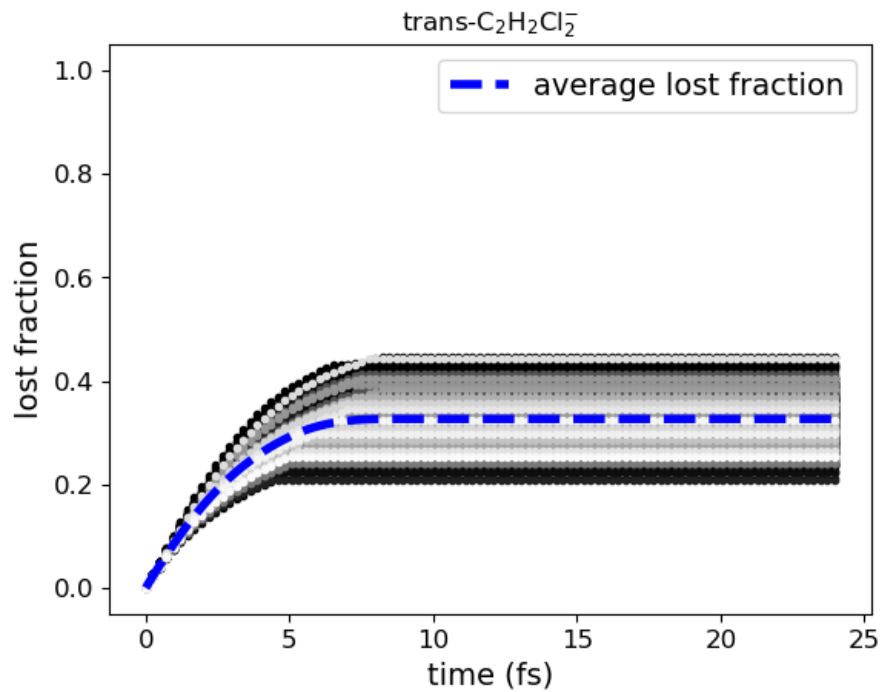
Figure 27: Lost fraction v time for *trans*-dichloroethylene anion.

1,1-dichloroethylene, C$_2$H$_2$Cl$_2$

Time step = 10 a.u. (0.2419 fs); Number of steps = 1000; Temperature = 350 K; Number of trajectories = 194; $\eta = 0.00010$ a.u.

Statistics on equilibrium lost fraction: *minimum*= 0.7911; *maximum*=0.9990; *mean* =0.9338; *median*=0.9383; *standard deviation* = 0.0482.
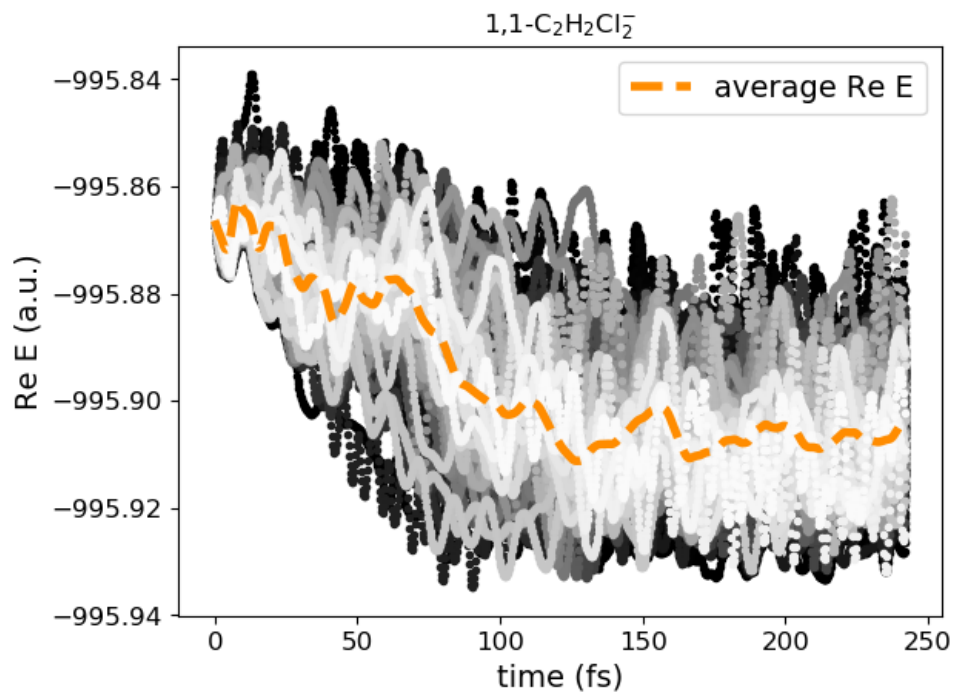
Figure 28: Re E v time for *cis*-dichloroethylene anion.
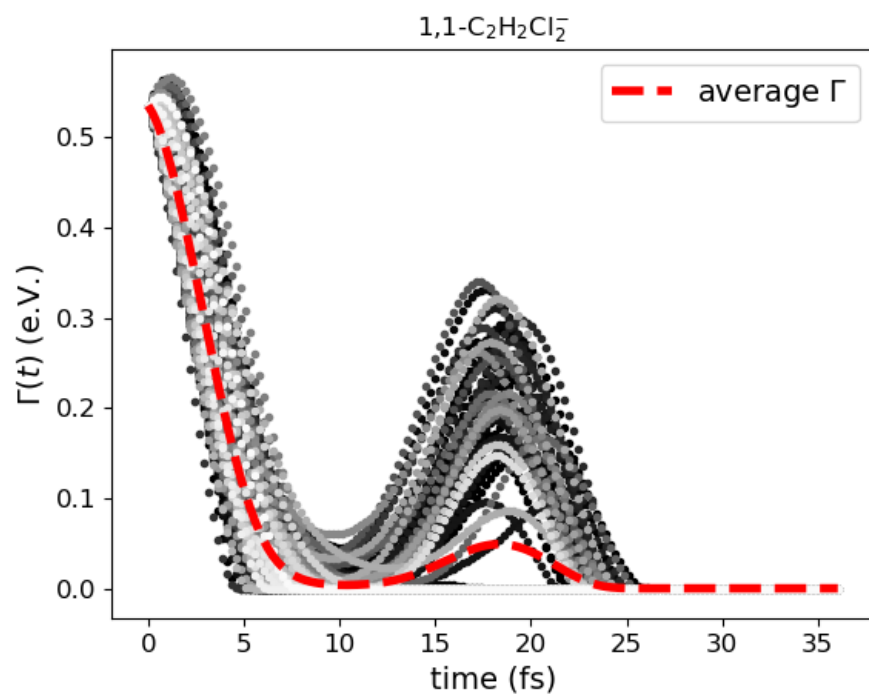
Figure 29: Resonance width, Γ, v time for *cis*-dichloroethylene anion.
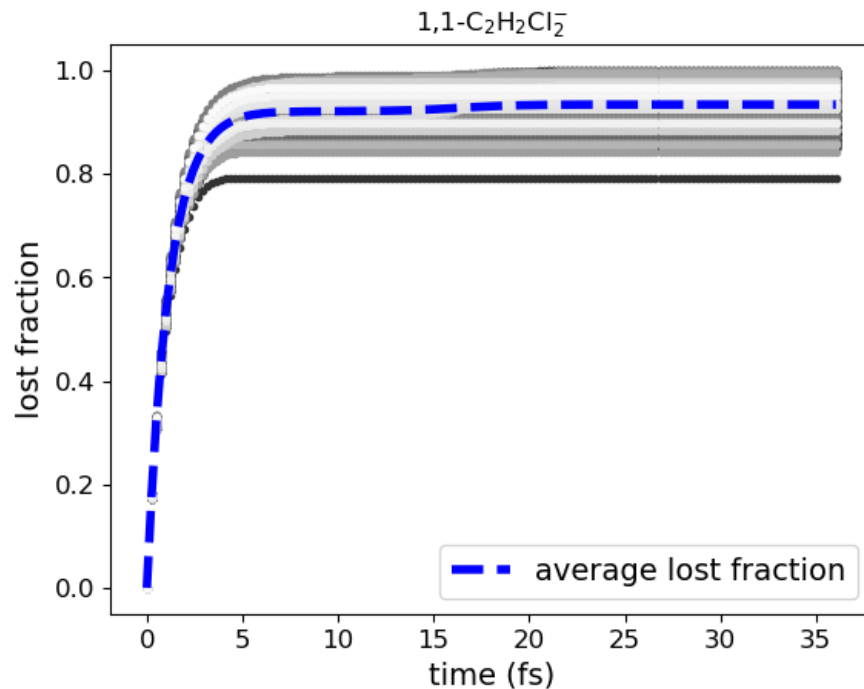
Figure 30: Lost fraction v time for *cis*-dichloroethylene anion.

On the out-of-plane motion of the dichloroethylene anion isomers

The top row graphs in Fig. 31 report the dihedral angle between the plane containing the two C atoms and: i) the dissociating Cl, and ii) the other non-C atom geminal to the dissociating Cl atom. The normal vectors of these two planes are defined such that they are anti-parallel to each other at $t = 0$. We observe from the dihedral plots that right from the onset of their time evolutions these ethylene derivative TAs go through an inexorable decrease in the dihedral angle ϕ in question, accompanied by the R-Cl bond elongation, where Cl refers to the dissociating chlorine. In the vast majority of our simulations, we see the R-Cl bond contracts just a little bit in the beginning before elongating as ϕ decreases. With the exception of 1,1-dichloroethylene (column D of Fig. 31), we also see a wiggly but steep drop of ϕ towards zero once $90° \lesssim \phi \lesssim 120°$. When $90° \lesssim \phi \lesssim 120°$, the R structure is often almost perpendicular to the R-Cl bond; this is usually when we begin to see a sharp increase in the R-Cl bond length.

Overall, as shown in the same plots, the sharp decrease in ϕ in the first $90 - 120$ fs follows more or less the same trend in time as Re E. The Mulliken charge on the dissociating Cl also decreases rapidly (see second row in Fig. 31) in the same interval of time that ϕ drops sharply. Interestingly, the time step at which this charge begins to stabilize is the same point at which we see a stabilization in Re E.
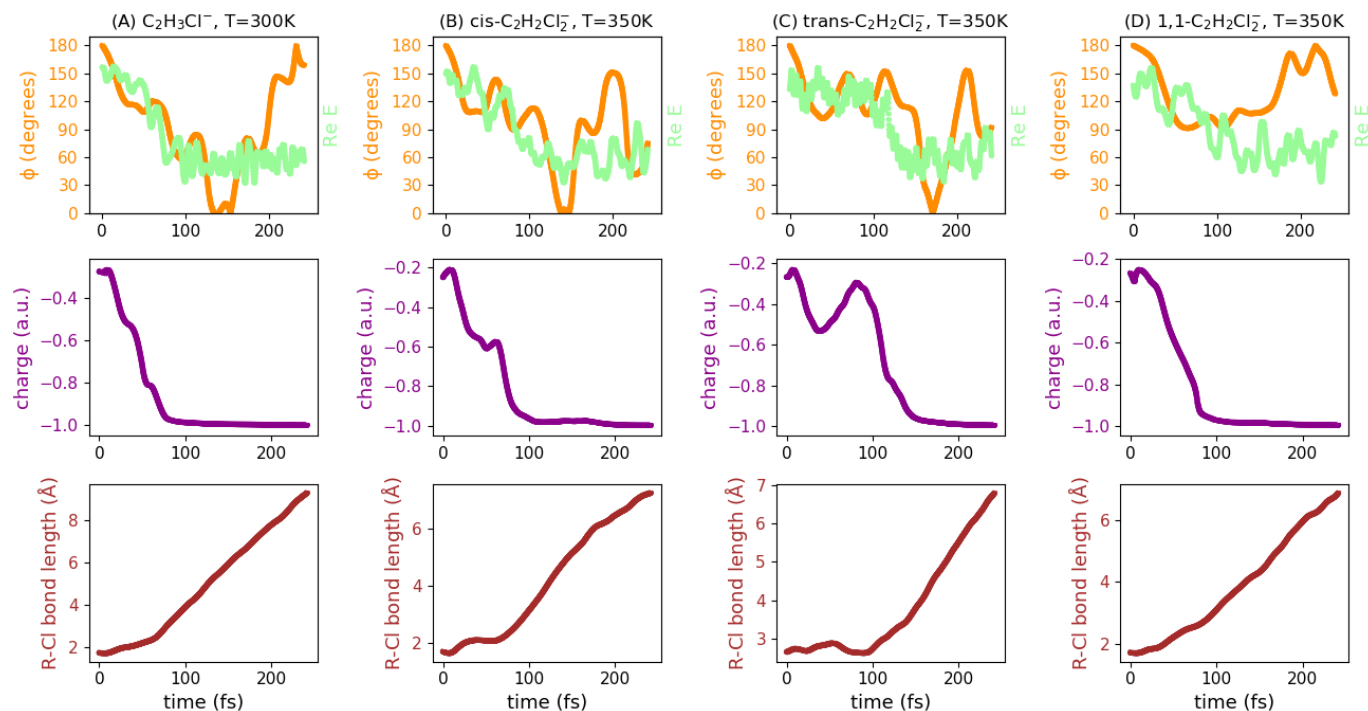
Figure 31: Dihedral angle, Mulliken charge (on dissociating Cl) and R-Cl bond length profiles for the trajectories shown in Fig. 3 of article (and Fig. 20 above).

Trichloroethylene, C_2HCl_3

We ran 24 trajectories, the dissociative electron attachment (DEA) process led to the formation of *trans*-dichloroethylene radical + Cl⁻ in 21 trajectories, *1,1*-dichloroethylene + Cl⁻ in 2 trajectories, and *cis*-dichloroethylene + Cl⁻ in 1 trajectory. We show below results for the first two channels. Results for the *cis*-dichloroethylene + Cl⁻ channel not shown below are very similar to the first two.

trans-dichloroethylene channel

Time step = 20 a.u. (0.4838 fs); Number of steps = 1000; Temperature = 370 K; Number of trajectories = 21; $\eta = 0.00500$ a.u.

Statistics on equilibrium lost fraction: _minimum_= 0.0861; _maximum_=0.2229; _mean_ =0.1148; _median_=0.1037; _standard deviation_ = 0.0389.
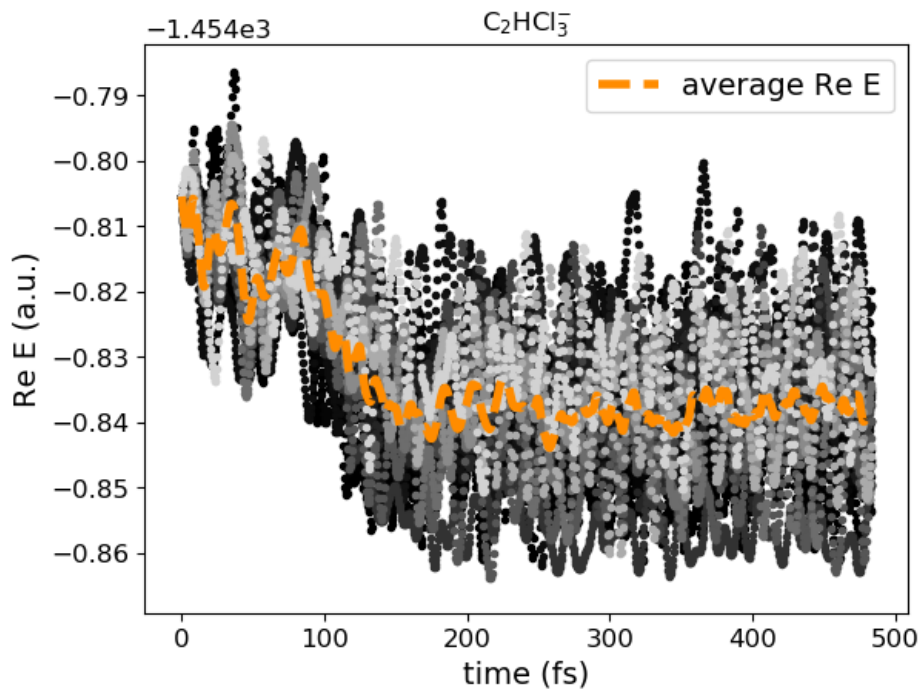
Figure 32: Re E v time for trichloroethylene anion. An offset of -1454.0 is used for the y-axis.
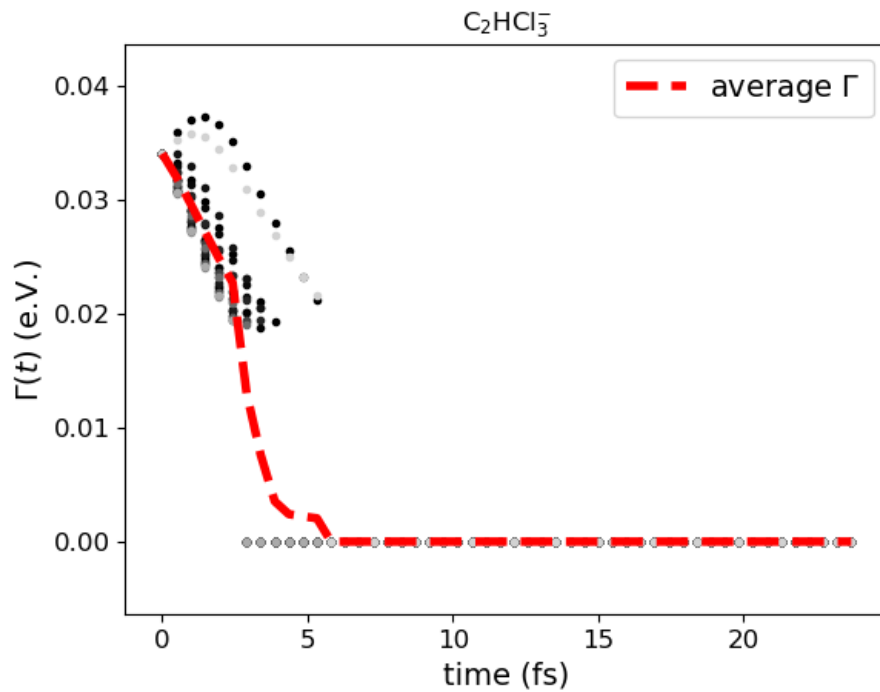
Figure 33: Resonance width, Γ, v time for trichloroethylene anion.
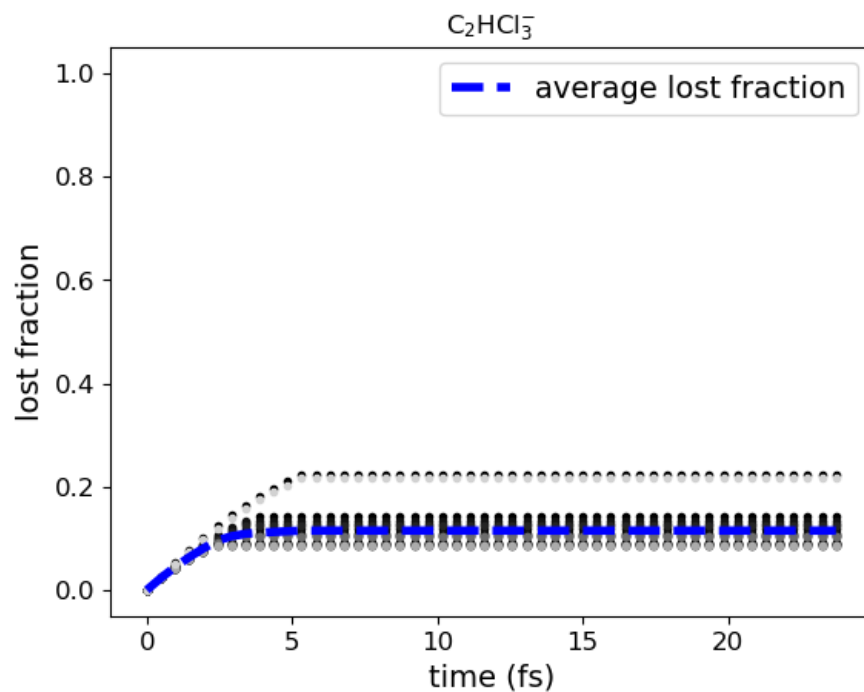
Figure 34: Lost fraction v time for trichloroethylene anion.

1,1-dichloroethylene channel

Time step = 20 a.u. (0.4838 fs); Number of steps = 1000; Temperature = 370 K; Number of trajectories = 2; $\eta = 0.00500$ a.u.
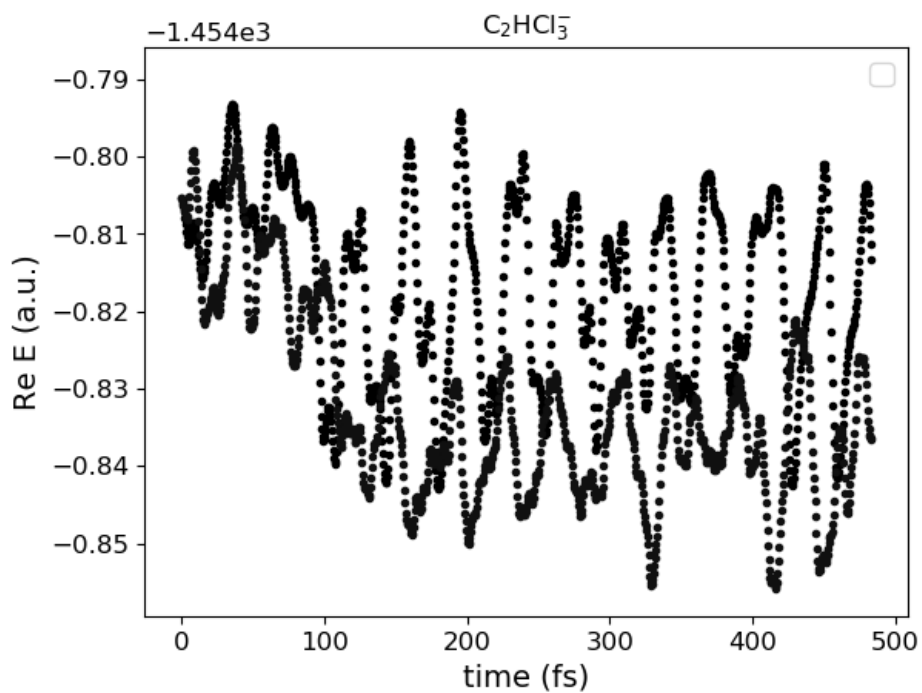
Figure 35: Re E v time for trichloroethylene. An offset of -1454.0 is used for the y-axis.
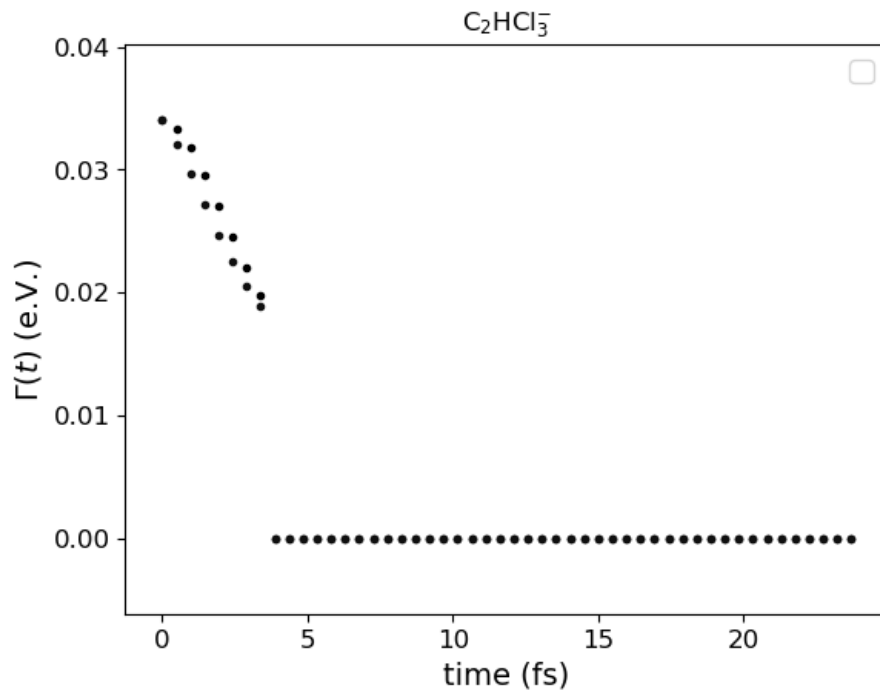
Figure 36: Resonance width, Γ, v time for trichloroethylene anion.
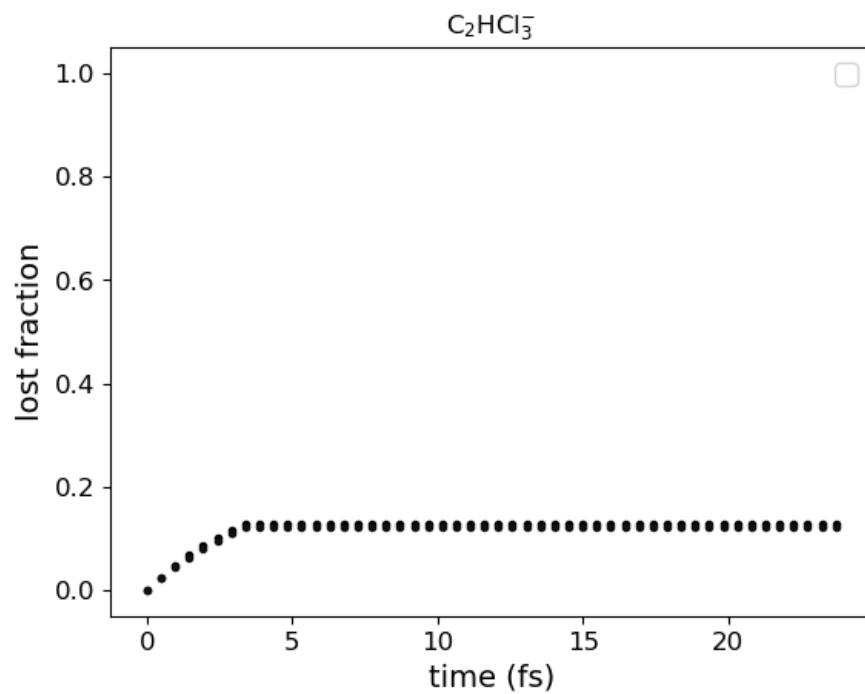
Figure 37: Lost fraction v time for trichloroethylene anion.

Tetrachloroethylene, C_2Cl_4

Time step = 20 a.u. (0.4838 fs); Number of steps = 1000; Temperature = 410 K; Number of trajectories = 21; $\eta = 0.02340$ a.u.

Statistics on equilibrium lost fraction: *minimum*= 0.0052; *maximum*=0.0053; *mean* =0.0053; *median*=0.0053; *standard deviation* = $3.71 \cdot 10^{-5}$.

The Γ profile here, Fig. 39, shows a very small width for the anion. Also, the width becomes zero almost immediately, i.e., after 1 fs. This is the reason why this particular DEA can be simulated without CAP. This observation is also in agreement with the very low lost fraction that we get from our simulations, see Fig. 40.
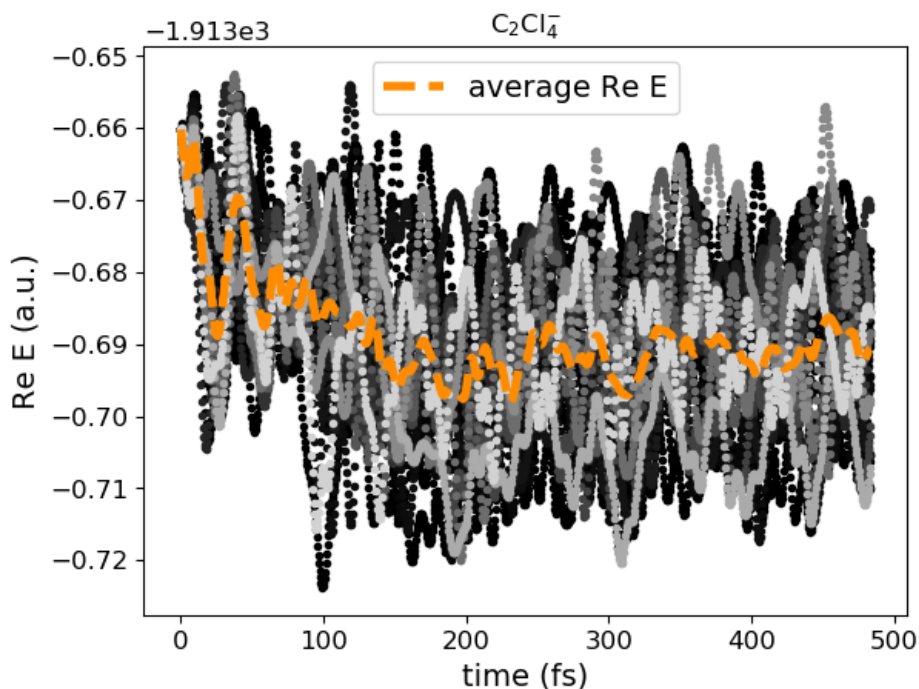
Figure 38: Re *E* v time for tetrachloroethylene anion. An offset of −1913.0 is used for the y-axis.
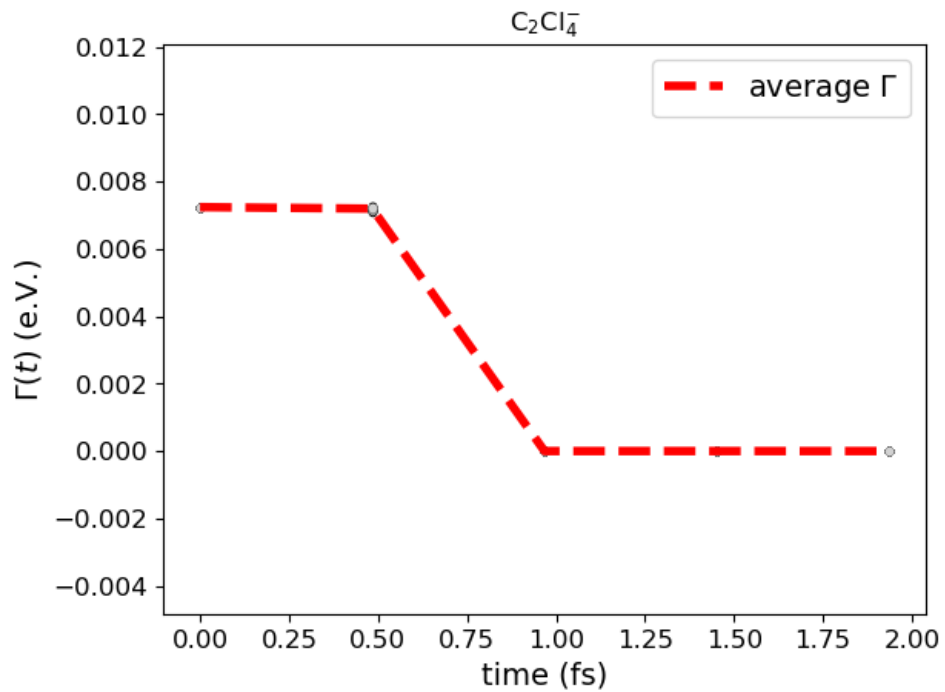
Figure 39: Resonance width, Γ, v time for tetrachloroethylene anion.
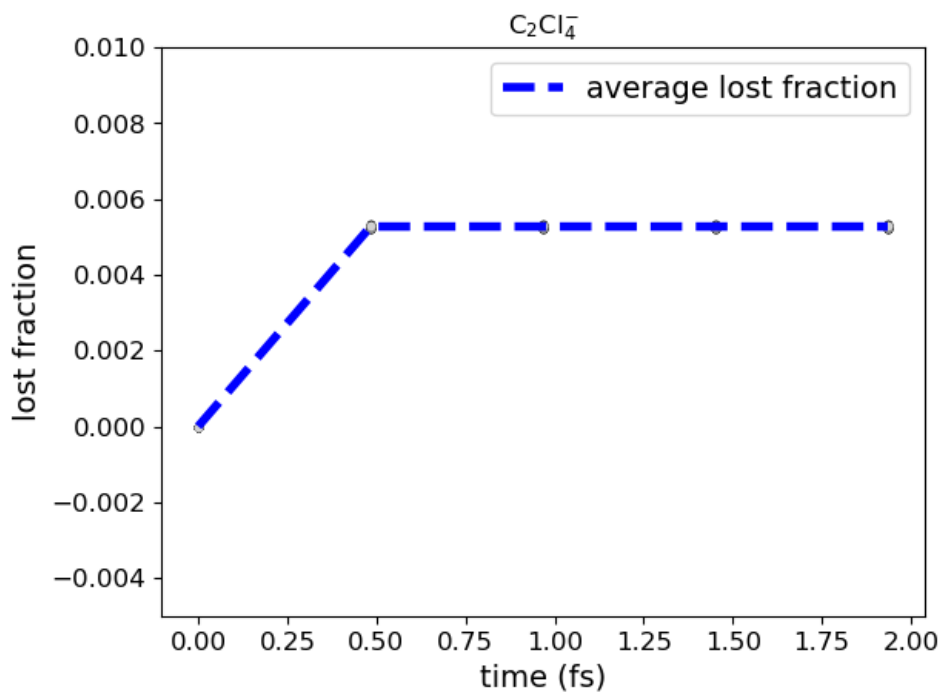
Figure 40: Lost fraction v time for tetrachloroethylene anion.

Chloroethane, C_2H_5Cl

Time step = 5 a.u. (0.1209 fs); Number of steps = 1200; Temperature = 260 K; Number of trajectories = 67.

The resonance width for chloroethane anion is higher compared to the chlorinated ethylene anions discussed above because we are dealing with a σ^* resonance here. We observe a very sharp rise of the lost fraction in the beginning. The average equilibrium lost fraction, $\langle f_\infty \rangle$, is practically unity, indicating that the DEA process for chloroethane anion is very inefficient. This is supported by experimental results.[10]
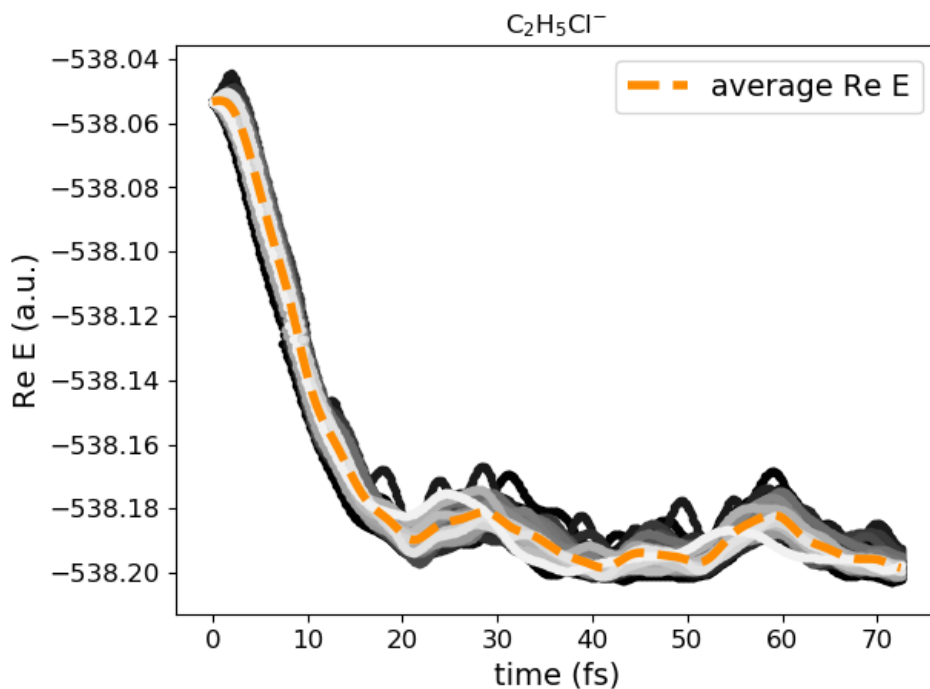
Figure 41: Re E v time for chloroethane anion.
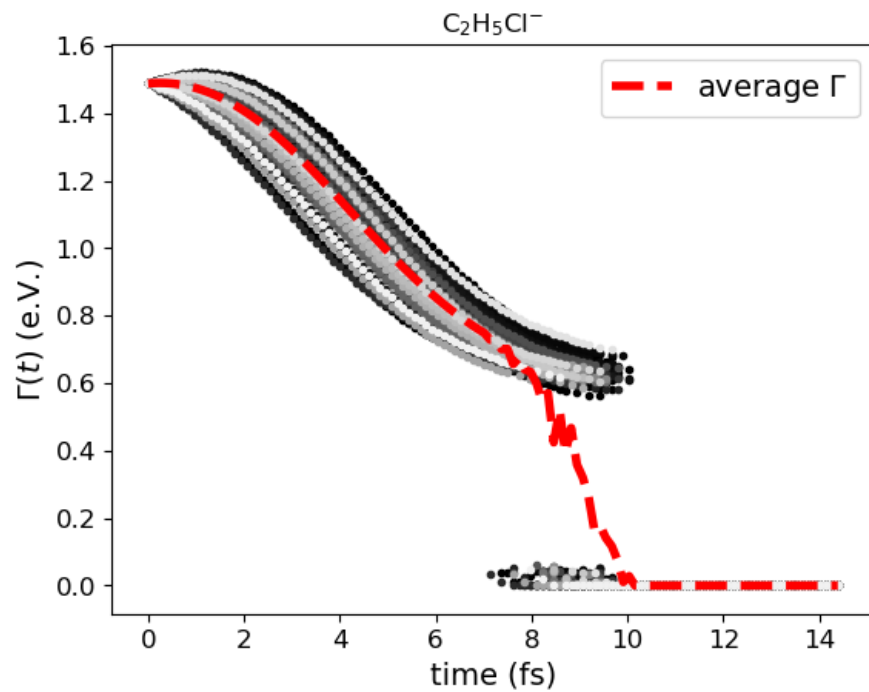
Figure 42: Resonance width, Γ, v time for chloroethane anion.
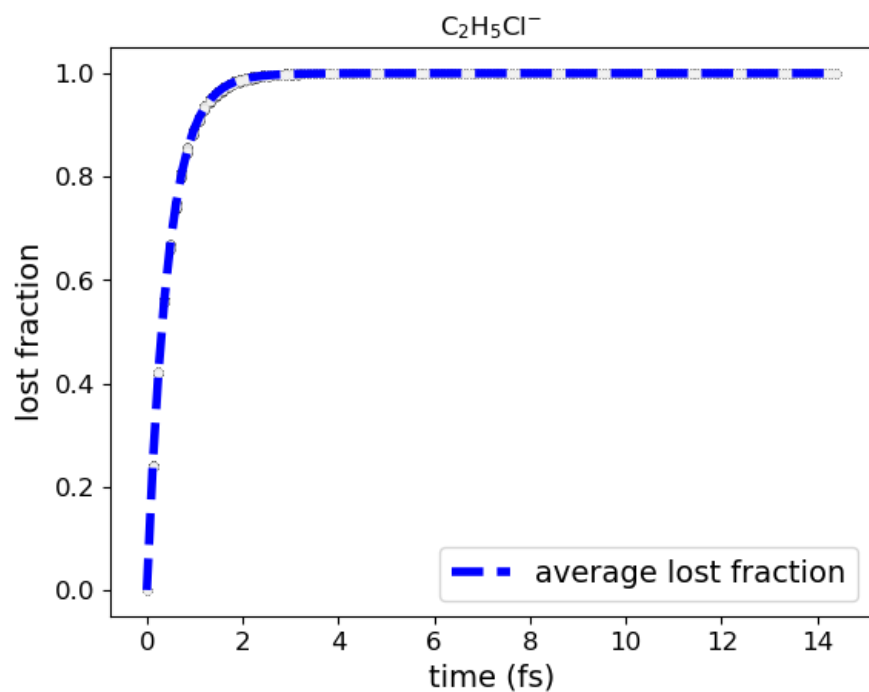
Figure 43: Lost fraction v time for chloroethane anion. The equilibrium lost fraction is ~ 1 for all trajectories.

References

(1) Riss, U. V.; Meyer, H. D. Calculation of resonance energies and widths using the complex absorbing potential method. *J. Phys. B: At. Mol. Opt. Phys.* **1993**, *26*, 4503–4535.

(2) Sommerfeld, T.; Riss, U. V.; Meyer, H.-D.; Cederbaum, L. S.; Engels, B.; Suter, H. U. Temporary anions - calculation of energy and lifetime by absorbing potentials: the resonance. *J. Phys. B: At. Mol. Opt. Phys.* **1998**, *31*, 4107–4122.

(3) Santra, R.; Cederbaum, L. S. An efficient combination of computational techniques for investigating electronic resonance states in molecules. *J. Chem. Phys.* **2001**, *115*, 6853–6861.

(4) Zuev, D.; Jagau, T.-C.; Bravaya, K. B.; Epifanovsky, E.; Shao, Y.; Sundstrom, E.; Head-Gordon, M.; Krylov, A. I. Complex absorbing potentials within EOM-CC family of methods: Theory, implementation, and benchmarks. *J. Chem. Phys.* **2014**, *141*, 024102.

(5) Dempwolff, A. L.; Hodecker, M.; Dreuw, A. Vertical ionization potential benchmark for unitary coupled-cluster and algebraic-diagrammatic construction methods. *J. Chem. Phys. 156*, 054114.

(6) Benda, Z.; Jagau, T.-C. Analytic gradients for the complex absorbing potential equation-of-motion coupled-cluster method. *J. Chem. Phys.* **2017**, *146*, 031101.

(7) Jagau, T.-C.; Zuev, D.; Bravaya, K. B.; Epifanovsky, E.; Krylov, A. I. A Fresh Look at Resonances and Complex Absorbing Potentials: Density Matrix-Based Approach. *J. Phys. Chem. Lett.* **2014**, *5*, 310–315.

(8) Benda, Z.; Jagau, T.-C. Understanding Processes Following Resonant Electron Attachment: Minimum-Energy Crossing Points between Anionic and Neutral Potential Energy Surfaces. *J. Chem. Theory Comput.* **2018**, *14*, 4216–4223.

(9) Burrow, P.; Modelli, A.; Chiu, N.; Jordan, K. Temporary Σ and Π anions of the chloroethylenes and chlorofluoroethylenes. *Chem. Phys. Lett.* **1981**, *82*, 270–276.

(10) Pearl, D. M.; Burrow, P. D. Dissociative attachment in selected monochloroalkanes. *J. Chem. Phys.* **1994**, *101*, 2940–2948.